Copyright is owned by the Author of the thesis. Permission is given for a copy to be downloaded by an individual for the purpose of research and private study only. The thesis may not be reproduced elsewhere without the permission of the Author.

Icy tornadoes in the quantum world - Josephson junctions of Bose-Einstein condensates

A thesis presented in partial fulfilment of the requirements
for the degree of

Master of Science
in
Mathematical Physics

at

Centre for Theoretical Chemistry and Physics,
New Zealand Institute for Advanced Study,
Massey University, Albany,
New Zealand.

Gabriele **JARITZ**

Auckland,
June, 7, 2012

Abstract

This thesis presents a theoretical study of ultra-cold gases in, or close to a Bose-Einstein condensed phase. A system of two coupled Bose-Einstein condensates shows strong resemblance to Josephson junctions, consisting of two superconductors linked via a thin insulating barrier. In these systems quantised ring currents across the barrier (Josephson vortices) have been detected. We concentrate on similar macroscopic quantum states in our systems of linear and annular coupled Bose-Einstein condensates, and test them towards their potential for showing macroscopic quantum tunnelling.

For the linear system we present a very detailed stability analysis of the stationary solutions, the vortex and the soliton, using Bogoliubov-de Gennes theory. An analytic approximation of the unstable mode is provided. We show that the transition between vortices rotating in opposite directions is possible and propose an effective potential separating these two states. For the annular system of two coupled ring shaped condensates of different radii, we review the parameter regimes for finding vortices in the ground state. We show that pinning of vortices via a repulsive external potential is possible and suggest further steps towards the detection of macroscopic quantum tunnelling.

Acknowledgements

I would like to thank my supervisor Joachim Brand for offering me the possibility to work on an interesting topic in his group, for all the fruitful discussions and for proofreading my drafts.
Special thanks goes to Oleksandr Fialko whose passion for physics was truly inspiring and motivating. Thanks for the countless number of discussions and the thoughts you put into my work.
I am thankful for the financial support received from the Marsden fund which made a full time study possible. It also financed the participation at the VSSUP 2011 in Melbourne and the Dodd-Walls symposium 2011 in Dunedin.
Last but not least I would like to thank all my colleagues for their warm welcome to the group and the positive and friendly working environment. You turned my stay in New Zealand into one of the best times of my life.

Contents

List of Figures

List of Tables

Chapter 1

Introduction & basics

1.1 General overview

The theoretical discovery of Bose-Einstein condensation (BEC) dates back to 1925 when A. Einstein predicted a phase transition in a gas of non-interacting atoms: due to quantum statistics all particles will end up in the ground state when cooled to a very low temperature. Although in real systems interactions are always present to some degree, the formation of a BEC is not restricted to the particular case of non-interacting particles. Indeed, the connection to superfluid ^4He, which is a strongly interacting system, was already made in 1938 by London [1] and today, Bose-Einstein condensation is believed to be one of the underlying mechanisms of superfluidity. Despite this early discovery, it needed the invention of laser techniques to sufficiently trap and cool the atom clouds, in order to experimentally realise a BEC in the lab. This was first achieved in 1995 with a gas of dilute alkali atoms [2]. The study of ultra-cold gases, in particular Bose-Einstein condensates (BEC) is an interesting topic from various aspects. Quantum phenomena are usually restricted to the microscopic world and are therefore hard to detect. Since a BEC confines a macroscopic number of particles in the same quantum state, it allows us to study quantum phenomena on a macroscopic scale, such as wave-particle duality and the tunnelling of macroscopic objects [3].

The substantial progress on magnetic and optical trapping techniques [4, 5] enables experimentalists nowadays to create condensates of various shapes, including lattices and systems of lower dimensionality. Although Bose-Einstein

condensation is impossible in homogeneous 1D and 2D systems (Hohenberg theorem [6]), it can be realised in atom traps where the density of states is altered by the confining potential. In weakly interacting, finite homogeneous systems, even if BEC does not strictly occur, the Gross-Pitaevskii mean-field theory of BECs yields reasonable approximations [7, 8]. We will study this regime and use the term BEC for low dimensional Bose systems in the sense that its mean field theory applies. Lower dimensional systems are of particular interest, not only because the computational effort of theoretical studies is reduced significantly, but also because they exhibit additional features, since the properties of phase transitions and the nature of collective excitations depend on the spatial degree of freedom. Quasi one-dimensional condensates were successfully realised in a number of experiments [9, 10, 11]. Dividing the condensate into two regions, by raising a potential barrier along one spatial dimension, allows the study of coupled BECs. Coherence between coupled BECs has been shown by Ketterle et al. [12, 13, 14], while a one-dimensional coupled system was recently realised by Schmiedmayer *et al.* [15, 16]. These systems show strong resemblance of Josephson junctions, consisting of two superconductors coupled via a thin insulating layer, where tunnelling of Cooper pairs (Josephson effect) is a well known phenomenon [17, 18, 19]. This analogy was pointed out by Smerzi *et al.* [20, 21, 22]. Experimental evidence of such tunnelling has been observed in short coupled BECs [23, 24], revealing features of point-like Josephson junctions. Increasing the 'contact area' of the two coupled superconductors generates long Josephson junctions (LJJ) for which Josephson fluxons are observed. A Josephson fluxon (Josephson vortex) is a ring current located in the middle of the tunnel barrier, producing a magnetic field with a quantised flux Φ_0. Similarly, one may also look for analogues of Josephson fluxons in extended coupled BECs [25, 26, 27]. Whether such effects like self trapping or Josephson oscillations are still observable in 1D Bose-Josephson junctions is the issue of an ongoing discussion [28, 29]. A very useful tool for a theoretical description of BECs is the famous Gross-Pitaevskii (GP) [30, 31] equation, also known as non-linear Schrödinger equation, which is formulated as a classical field theory using a mean field approximation for the particle-particle interaction. Interesting properties of the condensate, like the appearance of non-linear waves that keep their shape while propagating (solitons) and topologically stable quantised ring currents (vortices), can be studied within this theory as they are particular

solutions of the GP equation. Quantised vorticity has been studied in superconductors, superfluid helium and Bose-Einstein condensed ultra cold gases [32] and continues to be a fascinating subject for study. As mentioned, the mean field GP theory describes the classical features of the BEC, equivalent to the theory of electrodynamics describing the classical properties of photons in terms of the electromagnetic field. That means in order to describe quantum effects e.g. tunnelling, one has to go beyond this approximation. A very fruitful way of including quantum fluctuations numerically is a c-field technique known as the truncated Wigner method [33, 34, 35, 36, 37]. It includes quantum fluctuations in terms of noise by sampling over many trajectories in phase space, starting with modified initial conditions. In order to end up with meaningful results the choice of the relevant noise modes appears to be the crucial point in numerical simulations. Taking the modes of the elementary excitations, calculated by solving the Bogoliubov-de Gennes equations [30, 31], is the most accurate description known so far.

In our work we present two promising candidates for the study of macroscopic quantum tunnelling. In both cases a vortex is the macroscopic object of choice. In the first part we study two coupled cigar-shaped condensates where the strong confinement in the transverse dimensions allows for a one-dimensional description. We look at the stability of stationary solutions, namely dark solitons and fluxon analogs [38, 27], by solving the Bogoliubov-de Gennes equations. An analytical approximation for the unstable mode of the soliton is provided. Real time evolution confirms the existence of the soliton - vortex transition. We propose and motivate a very simple form of the effective potential of the vortex, which is crucial for further studies on vortex - antivortex tunnelling. The second part of this work deals with coupled ring shaped Bose-Einstein condensates in a one-dimensional description. We review the parameter regimes for which vortices appear and show the feasibility of pinning them with repulsive external potentials.

1.2 The Gross-Pitaevskii equation

In this section we give a derivation of the Gross-Pitaevskii equation (GPE) for one-dimensional systems. Although the result is the same for higher dimension-

ality, the argumentation has to be altered.
In order to describe a dilute gas at very low temperatures we aim to simplify the exact Hamiltonian of the system which, in terms of the field operator $\hat{\psi}$, reads

$$\hat{H} = -\frac{\hbar^2}{2m}\int dx\hat{\psi}^\dagger\partial_{xx}\hat{\psi} + \int dx\hat{\psi}^\dagger V_{\text{ext}}\hat{\psi} + \frac{1}{2}\int dxdx'\hat{\psi}^\dagger\hat{\psi}^\dagger V(x-x')\hat{\psi}\hat{\psi} \quad (1.1)$$

with $V(x)$ and $V_{\text{ext}}(x,t)$ being the two-body interaction and the external potential respectively. Using the Bose commutation relations

$$\left[\hat{\psi}(x'),\hat{\psi}(x)^\dagger\right] = \delta(x-x'), \qquad \left[\hat{\psi}^\dagger(x'),\hat{\psi}(x)^\dagger\right] = \left[\hat{\psi}(x'),\hat{\psi}(x)\right] = 0, \quad (1.2)$$

the Heisenberg equation of motion for the field operator can be deduced to give

$$\begin{aligned}\mathrm{i}\hbar\partial_t\hat{\psi}(x,t) &= \left[\hat{\psi}(x,t),\hat{H}\right] \\ &= \left(-\frac{\hbar^2}{2m}\partial_{xx} + V_{\text{ext}}(x,t) + \int dx'\hat{\psi}^\dagger(x',t)V(x-x')\hat{\psi}(x',t)\right)\hat{\psi}(x,t).\end{aligned} \quad (1.3)$$

To proceed further we need to make two approximations:

- ***Bogoliubov approximation***
  The field operators $\hat{\psi}(x)$ and $\hat{\psi}^\dagger(x)$ can be written in terms of the boson creation/annihilation operators $\hat{a}_i^\dagger$, $\hat{a}_i$ to give

  $$\hat{\psi}(x) = \sum_i \psi_i(x)\hat{a}_i, \qquad \hat{\psi}^\dagger(x) = \sum_i \psi_i^*(x)\hat{a}_i^\dagger, \quad (1.4)$$

  where $\psi(x)$, $\psi^*(x)$ are the c-number coefficients of the basis transformation. We continue by treating the ground state, denoted by the index 0, of the system separately and write the equations of (1.4) in the form

  $$\hat{\psi}(x) = \psi_0(x)\hat{a}_0 + \sum_{i>0}\psi_i(x)\hat{a}_i, \qquad \hat{\psi}^\dagger(x) = \psi_0^*(x)\hat{a}_0^\dagger + \sum_{i>0}\psi_i^*(x)\hat{a}_i^\dagger. \quad (1.5)$$

  The operators $\hat{a}_i$ and $\hat{a}_i^\dagger$ are defined by their effect on a number state

$|N\rangle = |N_0, N_1, N_2...\rangle$ which reads

$$\begin{aligned} \hat{a}_i|N_0...N_i...\rangle &= \sqrt{N_i}|N_0...N_i - 1...\rangle, \\ \hat{a}_i^\dagger|N_0...N_i...\rangle &= \sqrt{N_i + 1}|N_0...N_i + 1...\rangle, \end{aligned} \tag{1.6}$$

with $N_0, N_1, N_2...$ being the number of particles in the respective state.

Dilute gases at low temperatures confine a macroscopic fraction of particles in the ground state, e.g. $N_0 \gg 1$. Again, this is not strictly true but can be justified for the parameter regime we are looking at [7, 8]. That validates the Bogoliubov approximation

$$\begin{aligned} \hat{a}_0|N_0...N_i...\rangle &\approx \sqrt{N_0}|N_0...N_i...\rangle, \\ \hat{a}_0^\dagger|N_0...N_i...\rangle &\approx \sqrt{N_0}|N_0...N_i...\rangle, \end{aligned} \tag{1.7}$$

which replaces the creation/annihilation operators $\hat{a}_0^\dagger$, $\hat{a}_0$ with the c-number $\sqrt{N_0}$ assuming that a small change in particle number can be neglected, e.g. $N_0 + 1 \approx N_0$ and $N_0 - 1 \approx N_0$. This is equivalent to treating the condensed component as a classical field and writing equations (1.5) as

$$\hat{\psi}(x) = \psi(x) + \delta\hat{\phi}(x), \qquad \hat{\psi}^\dagger(x) = \psi^*(x) + \delta\hat{\phi}^\dagger(x), \tag{1.8}$$

where ψ is the wave function of the condensate and $\delta\hat{\phi}$ describes the quantum fluctuations in the system. Neglecting the second part of equation (1.8) the system behaves like a classical field.

- ***Pseudo-potential approximation***
  This approximation replaces the interaction between particles $V(x)$ with a contact interaction of the form

$$V(x - x') = g\delta(x - x'). \tag{1.9}$$

  While this approach holds in the 1D case, the pseudo-potential looks different in 3D [39].

Applying the above approximations and ignoring quantum and thermal deple-

tion of the condensate, we end up with the Gross-Pitaevskii equation [30, 40]

$$\mathrm{i}\hbar\partial_t\psi(x,t) = \left(-\frac{\hbar^2}{2m}\partial_{xx} + V_{\mathrm{ext}}(x,t) + g\left|\psi(x,t)\right|^2\right)\psi(x,t), \tag{1.10}$$

with the 1D non-linear interaction parameter $g = -2\hbar^2/ma$, written in terms of the 1D s-wave scattering length a [41]. The wave function (order parameter) ψ is normalised to the total number of particles in the system $\int|\psi(x)|^2dx = N$. As mentioned before, the GP equation provides a classical description of the system since no quantum fluctuations are included.

A stationary form of the GP equation can be found by writing the wave function as a product of a time-dependent and a time-independent part

$$\psi(x,t) = \psi(x)\mathrm{e}^{-\mathrm{i}\mu t/\hbar}, \tag{1.11}$$

where μ is the chemical potential, giving the average energy for adding a particle to the system. Substituting equation (1.11) into equation (1.10) yields the time-independent Gross-Pitaevskii equation

$$\left(-\frac{\hbar^2}{2m}\partial_{xx} + V_{\mathrm{ext}}(x) - \mu + g\left|\psi(x)\right|^2\right)\psi(x) = 0. \tag{1.12}$$

1.2.1 Continuity equation & velocity

We derive the continuity equation which leads to an expression for the velocity of the condensate. Multiplying equation (1.10) by ψ^* and subtracting the complex conjugate of the result, only the terms containing derivatives survive and we get

$$\begin{aligned}\mathrm{i}\hbar\left(\psi^*\partial_t\psi + \psi\partial_t\psi^*\right) + \frac{\hbar^2}{2m}\left(\psi^*\partial_{xx}\psi - \psi\partial_{xx}\psi^*\right) &= 0\\ \frac{\partial\left|\psi\right|^2}{\partial t} + \partial_x\left[\frac{\hbar}{2m\mathrm{i}}\left(\psi^*\partial_x\psi - \psi\partial_x\psi^*\right)\right] &= 0.\end{aligned} \tag{1.13}$$

Introducing $n = \left|\psi\right|^2$ as the number density, the upper equation can be written as

$$\frac{\partial n}{\partial t} + \partial_x\left(nv\right) = 0, \tag{1.14}$$

which uses the definition of the velocity

$$v = \frac{\hbar}{2m\mathrm{i}} \frac{(\psi^* \partial_x \psi - \psi \partial_x \psi^*)}{|\psi|^2}. \tag{1.15}$$

Describing the wave function in terms of the amplitude $\sqrt{n}$ and phase ϕ as $\psi(x) = \sqrt{n}\exp(\mathrm{i}\phi(x))$, equation (1.15) can be written as

$$v = \frac{\hbar}{m} \partial_x \phi. \tag{1.16}$$

Therefore, a spatial variation of the phase of the wave function indicates a flow in the condensate. Further reading can be found in [31].

1.3 Solitons in repulsive Bose-Einstein condensates

The time-dependent GP equation (1.10) has special solutions called solitons. For repulsive interaction, a soliton corresponds to a dip in the density (grey solitons) which moves along the condensate at constant velocity while conserving the shape of the density depression. This effect is a direct consequence of the non-linearity of the system. The depth of the dip depends on the velocity of the soliton, reaching zero density for zero velocity (dark soliton). For that, dark solitons are stationary solutions and solve equation (1.12). Solitons can also be characterised by the behaviour of the phase which undergoes a finite change over the condensate. For dark solitons, the otherwise smooth function $\phi(x)$, becomes steplike and reaches the value of π.
The analytic solution for the soliton was first derived by Tsuzuki [42] and reads:

$$\psi_0(x - vt) = \sqrt{n} \left(\mathrm{i}\frac{v}{c} + \sqrt{1 - \frac{v^2}{c^2}} \tanh \left[\frac{x - vt}{\sqrt{2}\xi} \sqrt{1 - \frac{v^2}{c^2}} \right] \right). \tag{1.17}$$

Here v is the velocity of the soliton, c the sound velocity and ξ the healing length. The latter is defined as $\xi = \hbar/\sqrt{2m\mu}$ and we think of the healing length as the distance over which the condensate returns to its bulk value when subject to a localized perturbation.

1.4 The Bogoliubov-de Gennes equations

The GP equation is a purely classical description of the system that doesn't include quantum fluctuations. One way of calculating the elementary excitation spectrum is to start from the GP equation (1.10) and introduce a small deviation $\delta\psi(x,t)$ in the condensate wave function of the unperturbed state. Although, we treat the fluctuations classically, not as field operators, they can be interpreted in terms of the elementary excitations of the system [30].

We wish to find solutions which are periodic in time apart from an overall phase factor and therefore make the Bogoliubov ansatz [30, 31]

$$\delta\psi(x,t) = e^{-\mathrm{i}\mu t/\hbar}\left[u(x)e^{-\mathrm{i}\omega t} + v^*(x)e^{\mathrm{i}\omega t}\right], \tag{1.18}$$

where ω is the frequency of the excitation. The additional phase factor $e^{-\mathrm{i}\mu t/\hbar}$ cancels the effect of the phase of the initial state and therefore makes sure that the equations can be satisfied for all times. Substituting $\psi(x,t) \to \psi(x) + \delta\psi(x,t)$ in equation (1.10), using the Bogoliubov ansatz (1.18) and linearising the problem, yields the two coupled equations

$$\begin{aligned}\left(-\frac{\hbar^2}{2m}\partial_{xx} + V(x) + 2g\left|\psi\right|^2 - \mu - \hbar\omega\right)u(x) + g\psi^2 v(x) = 0\\ \left(-\frac{\hbar^2}{2m}\partial_{xx} + V(x) + 2g\left|\psi\right|^2 - \mu + \hbar\omega\right)v(x) + g\psi^{*2} u(x) = 0.\end{aligned} \tag{1.19}$$

They are referred to as Bogoliubov equations. Here $\psi(x)$ is the wave function of the unperturbed state and the functions $u(x)$, $v(x)$ are the excitation modes. The above equations can be written in the form of an eigenvalue problem for the eigenenergies $\epsilon = \hbar\omega$ and the eigenvectors (u,v). The eigenenergies give information about the stability of the wave function ψ: every complex eigenenergy corresponds to one dynamically unstable mode that leads to the decay of the initial state $\psi(x)$. In fact, the condition for dynamical stability reads [43]

$$\mathrm{Im}(\epsilon) = 0. \tag{1.20}$$

An entirely real spectrum denotes a stable solution in a sense, that there are no linear instabilities. The BdG equations do not account for nonlinear instabilities. While one can deduce significant information from the eigenvalues,

the shape of $u(x)$ and $v(x)$ is not unique. Every complex eigenvector can be multiplied by any c-number without altering the density operator. It can be chosen such to make the perturbation $\delta\psi(x)$ orthogonal to the unperturbed initial state $\psi(x)$ [43].

Note that the sign in equation (1.18) connecting the positive and negative frequency parts can be chosen arbitrarily. A minus sign changes the sign of the last term in both equations (1.19).

Chapter 2

Stability of stationary solutions in coupled BECs

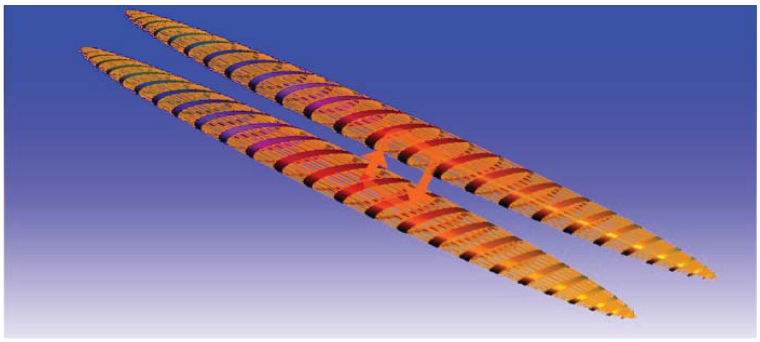

Figure 2.1: Sketch of two cigar-shaped Bose-Einstein condensates showing a ring current across the tunnel barrier.

In this section we investigate the stability of special solutions of the time-independent GP equation. We consider two cigar-shaped BECs which are coupled via tunnelling. The strong radial confinement allows for a one-dimensional description of the system. For linearly shaped one-dimensional BECs, we can revert to analytic expressions for the stationary soliton and vortex solutions [25]. Here, we use the term vortex to describe a localized ring current with quantized angular momentum going across the tunnel barrier region, as sketched in figure 2.1. The elementary excitations, causing the decay of the state, are described using Bogoliubov-de Gennes theory. Real time evolution shows the transition from a soliton to a vortex, allowing one to think of the vortex - antivortex tran-

sition as a valid scenario. We propose and try to justify a particular form of the effective potential for the vortex which allows for future studies on macroscopic quantum tunnelling of vortices. All numerical simulations are carried out using Matlab.

2.1 The coupled system

The Gross-Pitaevskii equations for two coupled, one-dimensional BECs in dimensionless units (see section B.1) reads [25, 26]

$$\mathrm{i}\partial_t\psi_j = -\frac{1}{2}\partial_{xx}\psi_j + |\psi_j|^2\psi_j - \psi_j - \nu\psi_{3-j}, \tag{2.1}$$

where ψ_j, $j = 1, 2$ are the classical fields describing the two BECs and ν is the tunnel coupling. To account for the linear shape of our system we use open boundaries that allow for arbitrary phases on the edges.
One stationary solution to equation (2.1) corresponds to a stationary dark soliton [25, 27]

$$\psi_{1,2} = \sqrt{1+\nu}\,\tanh(\sqrt{1+\nu}x). \tag{2.2}$$

The solutions in the two condensates coincide ($\psi_1 = \psi_2$) and the phase difference $\phi_2 - \phi_1$ is therefore zero (see figure 2.2). Although the soliton is stationary, it is not stable within a certain regime of the tunnel coupling, as we will see in section 2.2.
Another stationary configuration is the vortex, which can be written in the form

$$\psi_{1,2} = \sqrt{1+\nu}\,\tanh(2\sqrt{\nu}x) \pm \mathrm{i}\sqrt{1-3\nu}\,\mathrm{sech}(2\sqrt{\nu}x), \tag{2.3}$$

satisfying $\psi_1 = \psi_2^*$. It only exists in the regime of $\nu < 1/3$ where it turns out to be stable. The phase is a smooth function describing a flow in both condensates going in opposite directions. Therefore it can be interpreted as a vortex, e.g. a ring current going across the tunnel barrier, located at the position of the density dip. The properties of both solutions are visualised in figure 2.2.

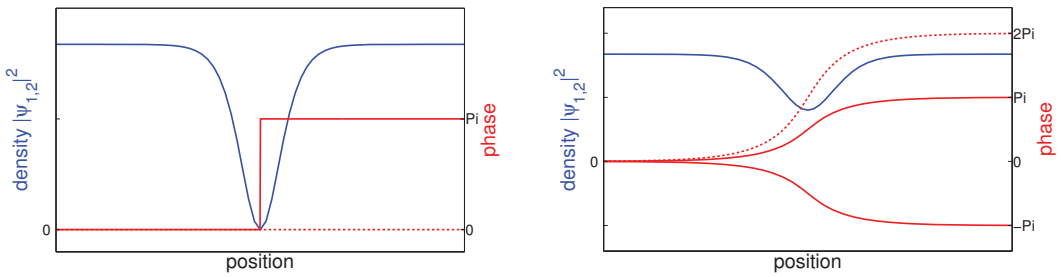

(a) (b)

Figure 2.2: (a) Illustration of a dark soliton in a linear, coupled Bose-Einstein condensate. (b) Illustration of the vortex solution in the same configuration. The full lines show the densities (blue) and the phases (red) along the condensate. The dotted line is the phase difference.

The energy in the system can be calculated from the functional

$$E[\psi_1, \psi_2] = \sum_{j=1}^{2} \int dx \left(\frac{1}{2} |\partial_x \psi_j(x)|^2 + \frac{1}{2} |\psi_j(x)|^4 - |\psi_j|^2 - \nu \psi_j^* \psi_{3-j} \right). \quad (2.4)$$

The energy of the homogeneous background ψ_j^0 has to be subtracted, in order to get a quantity independent of the system size. The wavefunctions $\psi_j^0 = \sqrt{n_j}$ are calculated separately for the two components keeping the particle number on its initial value for the state ψ_j, reading $N_j = \int dx \psi_j^* \psi_j$. The energy of the soliton and the vortex can be calculated analytically and is given by [25]

$$\text{soliton :} \qquad E_s = \frac{8}{3}(1+\nu)^{3/2} \quad (2.5)$$

$$\text{vortex :} \qquad E_v = \frac{8}{3}\sqrt{\nu}(3-\nu). \quad (2.6)$$

For the numerical evaluation of equation (2.4) we use a five-point stencil for the first derivative. The energy does not depend on the system size as long as the the wave function reaches its background density at the edges. A typical value for the system size is $L = [-10, 10]$ with $M = 101$ grid points, corresponding to $\Delta x = 0.2$. Using the notation $\psi(x) \to a_n$ with $x = -L + (n-1)\Delta x$ for $n = [1...M]$, our Neumann boundary conditions read $a_{-1} = a_0 = a_1$ and $a_{M+2} = a_{M+1} = a_M$. The result of both approaches is shown in figure 2.3.

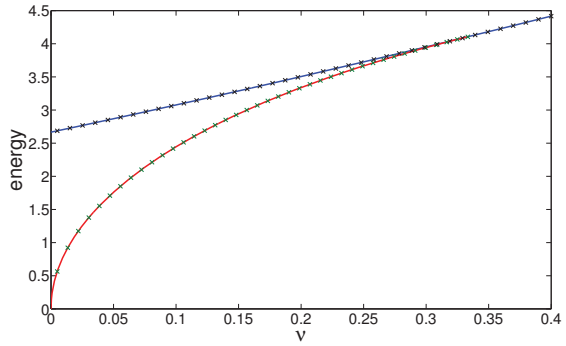

Figure 2.3: The energy of the soliton (blue) and the vortex (red) as a function of the tunnel coupling. The solid lines show the analytical results of equations (2.5), (2.6), the crosses are the numerical results calculated via equation (2.4).

2.2 Stability analysis

In order to analyse the stability of the stationary solutions of our coupled system, we write down the Bogoliubov-de Gennes (BdG) equations introduced in section 1.4. Based on the coupled GP equations (2.1) they read

$$\begin{pmatrix} D_1 - \epsilon & \psi_1^2 & -\nu & 0 \\ -\psi_1^{*2} & -D_1 - \epsilon & 0 & \nu \\ -\nu & 0 & D_2 - \epsilon & \psi_2^2 \\ 0 & \nu & -\psi_2^{*2} & -D_2 - \epsilon \end{pmatrix} \begin{pmatrix} u_1 \\ v_1 \\ u_2 \\ v_2 \end{pmatrix} = 0, \tag{2.7}$$

where $D_{1,2} = -\frac{1}{2}\partial_{xx} + 2\left|\psi_{1,2}\right|^2 - 1$ and $u_{1,2}, v_{1,2}$ are the excitation modes in the two condensates with energy ϵ. Before calculating the eigensystem numerically using Matlab, we need to adjust the analytical solution for the background (2.2) to our finite size system. Therefore we use Broyden's method to look for the roots of the GP equations (2.1), which is capable of finding local minima in the vicinity of a starting point. Expecting only small deviations from the soliton solution we start with equation (2.2) as an initial guess. Broyden's method is explained in section A.2.

The eigenvalues always come in pairs with opposite signs ($\pm$), since the BdG equation couples $\delta\psi$ and $\delta\psi^*$ (1.18). The spectrum for the soliton strongly depends on the parameter ν. In the regime of $0 < \nu < 1/3$ only one purely imaginary eigenvalue appears in the otherwise entirely real spectrum, representing a

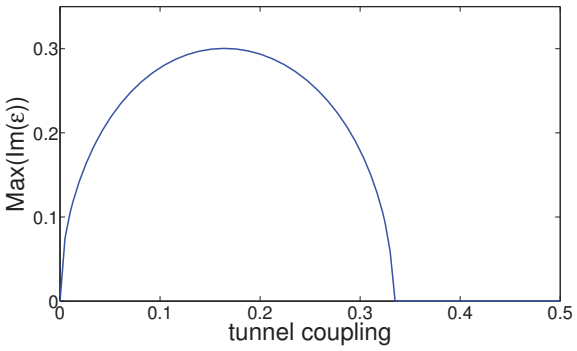

Figure 2.4: The non-vanishing imaginary part of one eigenvalue of the BdG equations indicates an unstable state.

single unstable mode. This is shown in figure 2.4. We spot two special points in the parameter regime of the tunnel coupling at $\nu = 0$ and $\nu = 1/3$. At $\nu = 1/3$ the soliton and vortex solution merge, which justifies the term exceptional point. The second one at $\nu = 0$ is special as well since the vortex vanishes and so does the instability of the soliton. Together we refer to them as critical points.
An imaginary eigenvalue also gives rise to a complex eigenvector. The components u_1, v_1 of the unstable mode for various tunnel coupling parameters are shown in figure 2.5. The modes in the second BEC turn out to be the negative of the first one, e.g. $u_1 = -u_2, v_1 = -v_2$ and are not shown here. Note that the shape of the real and imaginary components is not unique, since complex eigenvectors can always be multiplied by an arbitrary c-number.
The spectrum of the vortex (2.3) turns out to be entirely real, signifying a stable solution.

2.3 Analytical approximation of the unstable mode

The imaginary eigenenergy in the Bogoliubov spectrum of the soliton provides information about the instability of this state. When considering quantum tunnelling of vortices one has to specify the potential separating the two vortex states. It turns out that the curvature of the potential is determined by the energy of the unstable mode of the soliton. That motivated us to calculate this

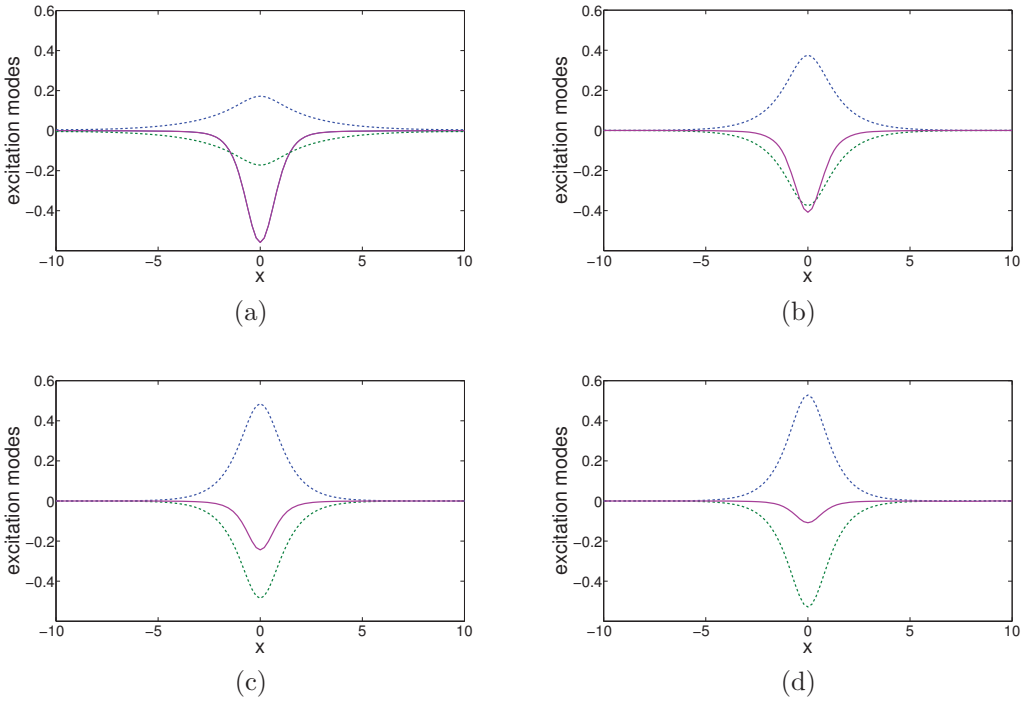

Figure 2.5: The unstable mode of the soliton for different values of the tunnel coupling constant ν. The dotted lines show the imaginary parts of u_1 (blue) and v_1 (green), the full (purple) line shows the real parts of u_1 and v_1. The parameters are (a) $\nu = 0.04$, $\epsilon = 0.1982$ (b) $\nu = 0.165$, $\epsilon = 0.3005$ (c) $\nu = 0.27$, $\epsilon = 0.2343$ (d) $\nu = 0.32$, $\epsilon = 01168$.

single mode analytically. In this section we present a new way of calculating analytically the single unstable mode of the soliton described in section 2.2. The exact solution of the BdG equations of a single BEC given by Sykes [44], has provided very useful inspiration.

Analysing the components of the unstable mode from our numerical calculations we find them to be highly symmetric (see figure 2.5). This validates the ansatz $u_1 = -u_2$, $v_1 = -v_2$, which reduces equation (2.7) to a 2×2 problem. Substituting $u_1 = u$ and $v_1 = v$ we get

$$\begin{pmatrix} D + \nu - \epsilon & \psi^2 \\ -\psi^2 & -D - \nu - \epsilon \end{pmatrix} \begin{pmatrix} u \\ v \end{pmatrix} = 0, \tag{2.8}$$

with $D = D_1 = D_2$. The tunnel coupling has the effect of shifting the chemical potential. From figure 2.5 we see that the unstable mode consists of a real and

$$(a)\quad \begin{array}{c||c} u_0 & N_0\cosh^{-2}(\sqrt{1+\nu}x) \\ u_{1/3} & N_1\cosh^{-1}(\sqrt{1+\nu}x) \\ \bar{u}_0 & u_0 \\ \bar{u}_{1/3} & N_4\left(u_{1/3}-N_3u_0\right) \end{array} \qquad (b)\quad \begin{array}{c||c} N_0 & \sqrt{3/4\sqrt{1+\nu}} \\ N_1 & \sqrt{1/2\sqrt{1+\nu}} \\ N_3 & \pi/4\sqrt{3/2} \\ N_4 & 1/\sqrt{1-N_3^2} \end{array}$$

Table 2.1: (a) Solutions for the modes at the critical points together with their orthogonalised versions. (b) Normalisation constants used within the analytical calculation.

an imaginary component, whereof one vanishes at the critical points $\nu = 0$, $\nu = 1/3$ respectively. That suggests to write the eigenfunction for arbitrary ν as a linear combination of the solutions at these two points. This is the main idea of the procedure presented below.

As a first step we describe a way of calculating analytical solutions for u and v at the critical points. Accounting for additional symmetry features $u = v$ at $\nu = 0$ and $u = -v$ at $\nu = 1/3$, both corresponding to $\epsilon = 0$, transforms equation (2.8) into two uncoupled Schrödinger equations with two different Rosen-Morse type potentials

$$\left[-\frac{1}{2}\partial_{xx} - (1+\nu)\frac{3}{\cosh^2(\sqrt{1+\nu}x)} + 2(1+2\nu)\right] u_0(x) = 0 \tag{2.9}$$

$$\left[-\frac{1}{2}\partial_{xx} - (1+\nu)\frac{1}{\cosh^2(\sqrt{1+\nu}x)} + 2\nu\right] u_{1/3}(x) = 0. \tag{2.10}$$

Here $u_0, u_{1/3}$ are the solutions at the corresponding critical points. Equations (2.9) and (2.10) can be solved analytically [45] by hypergeometric functions [46] providing us with the desired basis functions.
The obtained functions are not orthogonal, but because we end up with an eigenvalue problem, it is necessary to orthonormalise them. This is done by applying the Gram-Schmidt procedure. The functions $u_0, u_{1/3}$ together with the orthonormalised versions $\bar{u}_0, \bar{u}_{1/3}$ and all constants are given in table 2.1.

Knowing the basis functions, we continue with the procedure of rewriting

equation (2.8). We now define

$$f_+ = u + v \tag{2.11}$$
$$f_- = u - v, \tag{2.12}$$

which allows to write equation (2.8) in the simple form

$$H_+ f_+ = \epsilon f_- \tag{2.13}$$
$$H_- f_- = \epsilon f_+ \tag{2.14}$$

with $H_\pm = D + \nu \pm \psi^2$. Now, we write the modes as a linear combination of the orthogonalised solutions at the critical points

$$f_+ \;\; = a_+ \bar{u}_0 + b_+ \bar{u}_{1/3} \tag{2.15}$$
$$f_- \;\; = a_- \bar{u}_0 + b_- \bar{u}_{1/3}, \tag{2.16}$$

where $a_\pm, b_\pm$ are complex numbers. This is substituted into equation (2.14). When projecting onto the basis functions $\bar{u}_0, \bar{u}_{1/3}$ one has to evaluate overlap integrals of the form $< \bar{u}_{0,1/3} | H_\pm | \bar{u}_{0,1/3} >$ for all possible combinations. After straightforward calculations we end up with the following matrix

$$\begin{pmatrix} \frac{4}{5}\nu(-1+4\nu) & -\frac{1}{60}N_3N_4(1+\nu)\left(12\nu + N_4^2(1+\nu)\right) \\ -\frac{1}{5}N_3N_4(1+\nu)\nu & \frac{1}{60}\left(12\nu + N_4^2(1+\nu)\right)\left(-5+15\nu + N_3^2N_4^2(1+\nu)\right) \end{pmatrix} \begin{pmatrix} a_+ \\ b_+ \end{pmatrix} = \epsilon^2 \begin{pmatrix} a_+ \\ b_+ \end{pmatrix}. \tag{2.17}$$

This provides us with the imaginary eigenenergy and the coefficients a_+, b_+ defining the eigenmodes u, v. The analytical solution for the imaginary eigenvalue of interest of equation (2.17) reads

$$\epsilon = \Big\{ -\Big[\sqrt{8}(\nu+1)\left[405\nu(3\nu-1)\pi^6 - 72(371\nu^2 - 102\nu - 9)\pi^4 + 768(189\nu^2 - 34\nu - 15)\pi^2 + 2048(3\nu-5)^2\right]^{1/2} \\ - \; 135\nu(3\nu-1)\pi^4 + 24(373\nu^2 - 110\nu - 3)\pi^2 - 128(387\nu^2 - 98\nu - 5)\Big] / \left[15(3\pi^2 - 32)^2\right] \Big\}^{1/2}. \tag{2.18}$$

This can be approximated by

$$\epsilon = \sqrt{-(\nu+1)\sqrt{a\nu^2 + b\nu + c} + d\nu^2 + e\nu + f}, \tag{2.19}$$

with the parameters given in table 2.2.

a	b	c	d	e	f
18.5830	7.4328	0.6750	7.3877	4.2093	0.8216

Table 2.2: Parameters of the analytic solutions for the unstable mode of the soliton.

The missing coefficients are determined by

$$a_- = \frac{2\nu}{\epsilon} a_+, \qquad b_- = \frac{1}{\epsilon}\left(2\nu + N_4^2(1+\nu)/6\right) b_+. \tag{2.20}$$

It turns out that a_+, b_+ contribute to the real part of the solution, while a_-, b_- account for the imaginary part only. The original modes u, v can be calculated rearranging equations (2.12) and (2.16) to

$$u = \frac{1}{2}\left[(a_+ + a_-)\bar{u}_0 + (b_+ + b_-)\bar{u}_{1/3}\right] \tag{2.21}$$

$$v = \frac{1}{2}\left[(a_+ - a_-)\bar{u}_0 + (b_+ - b_-)\bar{u}_{1/3}\right]. \tag{2.22}$$

The results for the unstable mode show very good agreement with the numerical calculation of section 2.2. This is shown in figure 2.6.

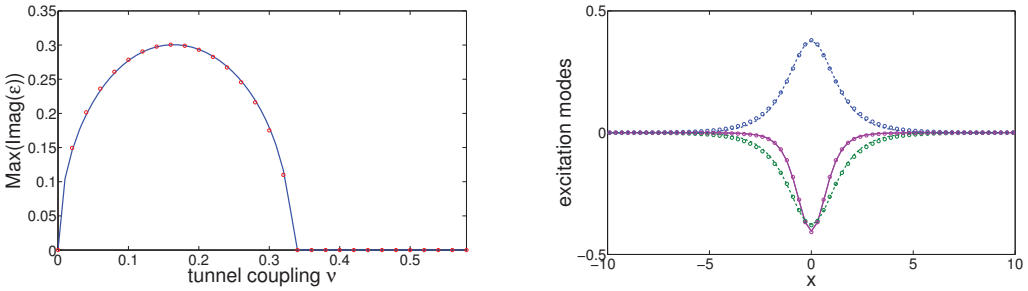

(a) (b)

Figure 2.6: Comparison of the analytical results (lines) with the numerical results (circles). (a) The imaginary eigenvalue of the BdG equation as a function of the tunnel coupling. Numerical results as in figure 2.4 (b) Real and imaginary parts of the unstable mode at $\nu = 0.167$, with the numerical result and colour allocation identical to figure 2.5.

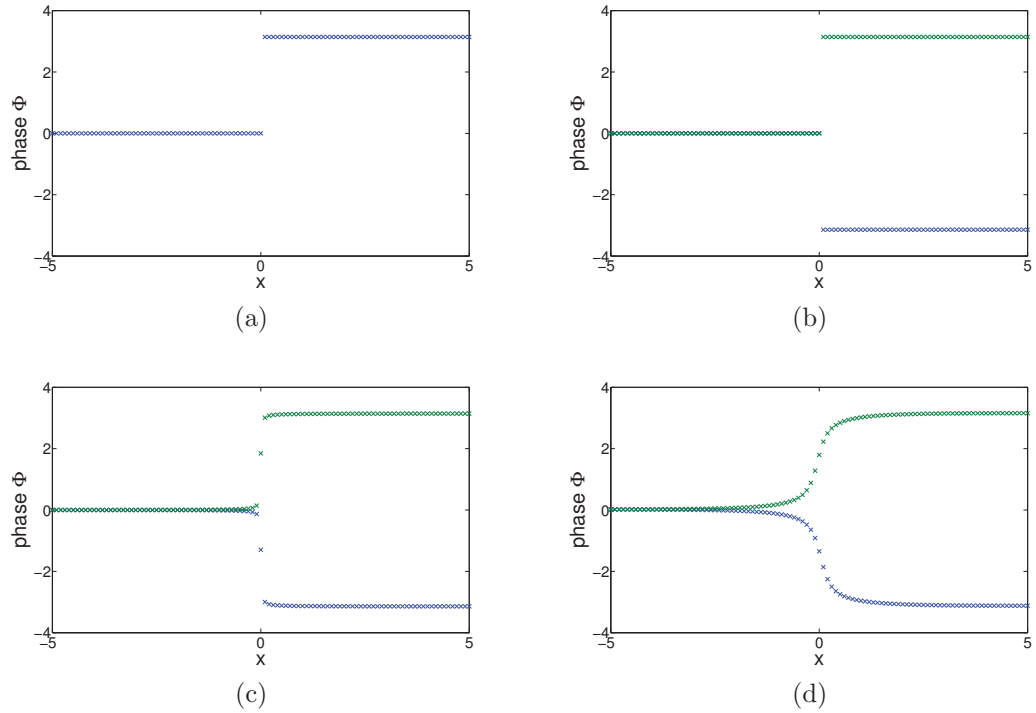

Figure 2.7: The phase of the two condensates during real time evolution, showing the transition from a soliton to a vortex. Tunnel coupling $\nu = 0.31$. (a) $t = 0$, (b) t=106 (c) t = 212, (d) t= 230.

2.4 Real time dynamics

In this section we study the behaviour of the system in real time. We solve the time-dependent GP equation (2.1) using the Matlab routine 'ode45', which is a Runge-Kutta method of order four. Starting from the stationary dark soliton we expect decay of the state, due to the existing unstable mode. This is discussed in detail in sections 2.2 and 2.3. We show that a continuous soliton-vortex and vortex-antivortex transition is possible [47], even within our classical model. The phase, as the identifying feature of the state, changes from a step function (soliton) to a smooth function (vortex), linking 0 and $\pm\pi$. This is shown in figure 2.7.

Because the shape of a function is hard to analyse, we look for a more convenient indicator. Therefore, we choose the momentum difference in the two condensates

$$\Delta P = \int (p_1 - p_2)\, dx, \tag{2.23}$$

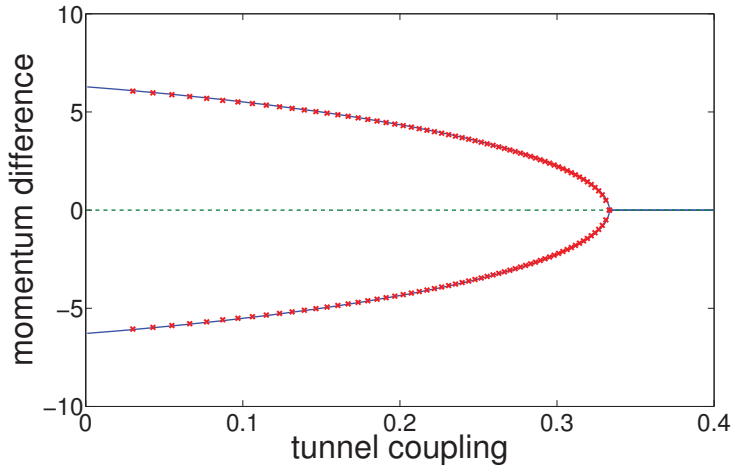

Figure 2.8: The momentum difference for the vortex and the soliton state in dimensionless units as a function of the tunnel coupling. The crosses show the numerical result for the vortex, the solid blue line gives the analytical results using (2.25). The soliton is represented by the dashed zero line.

with $p_j = -\mathrm{i}/2\left(\psi_j^*\nabla\psi_j - \psi_j\nabla\psi_j^*\right)$ being the momentum density in dimensionless units (see section B.1). This quantity is zero for the soliton state where both wave functions are the same and has a non-zero value for the existing ring current of the vortex state. We allot $\Delta P > 0$ to the vortex and $\Delta P < 0$ to the anti-vortex. The value of the momentum difference for the vortex depends on the tunnel coupling constant.

It is possible to find an analytical expression for the momentum difference of the vortex as a function of ν. For the vortex, equation (2.23) can be simplified to

$$\Delta P_V = 2\int_{-\infty}^{\infty} \mathrm{Im}(\psi_2\partial_x\psi_1)dx. \tag{2.24}$$

Using the known expressions of equation (2.3) for the vortex state, we find

$$\Delta P_V = \pm 2\pi\sqrt{1+\nu}\sqrt{1-3\nu}, \tag{2.25}$$

where the + sign corresponds to the vortex and the − sign to the antivortex. The numerical and analytical results are shown in figure 2.8.

The time evolution of this quantity is shown in figure 2.9 where, starting

with the soliton configuration, we see oscillations around the vortex state. The behaviour of the system is sensitive to its size and to the accuracy of the Runge-Kutta algorithm. The change from the vortex to the anti-vortex state is only encountered for a small system combined with low accuracy.

Looking at the density distribution in the condensate during the time evolution helps explain this finding. When performing the soliton-vortex transition, particles have to be shovelled into the region of the density regression. This happens by stimulating elementary excitations in form of phonons, which move through the condensate with constant velocity until they are reflected on the boundaries of the computational box. This can be seen in figure 2.10.

In the smaller system it is more likely to find the energy recombined in the area of interest, which helps to overcome the soliton barrier and end up with the antivortex state, while in the larger system it spreads over a wider region. The local energy along with the total energy for a large system is shown in figure 2.11. Nevertheless, a vortex-antivortex oscillation is only encountered for low accuracy of the Runge-Kutta method where particle number and total energy are not sufficiently conserved. Since such imperfections are always part of the experimental reality (finite temperature, trap noise...), oscillations may occur readily in experiments. As mentioned, the above simulations are purely classical, since no quantum fluctuations are included.

For the purpose of simulating quantum tunnelling of vortices in an infinite system we want to avoid reflected phonons from the edges. Therefore the simulation can only be run until the time the first phonons reach the area of the vortex again. This problem may be overcome by implementing absorbing boundaries conditions.

2.5 Modelling the potential

In order to study vortex - antivortex tunnelling, it is crucial to parametrize the effective potential separating these two states. The potential we are looking for, should show minima for the vortex and antivortex and a saddle point for the soliton. The shape of a potential separating two macroscopic quantum states can often be pictured as a double well as shown in figure 2.12, and written in

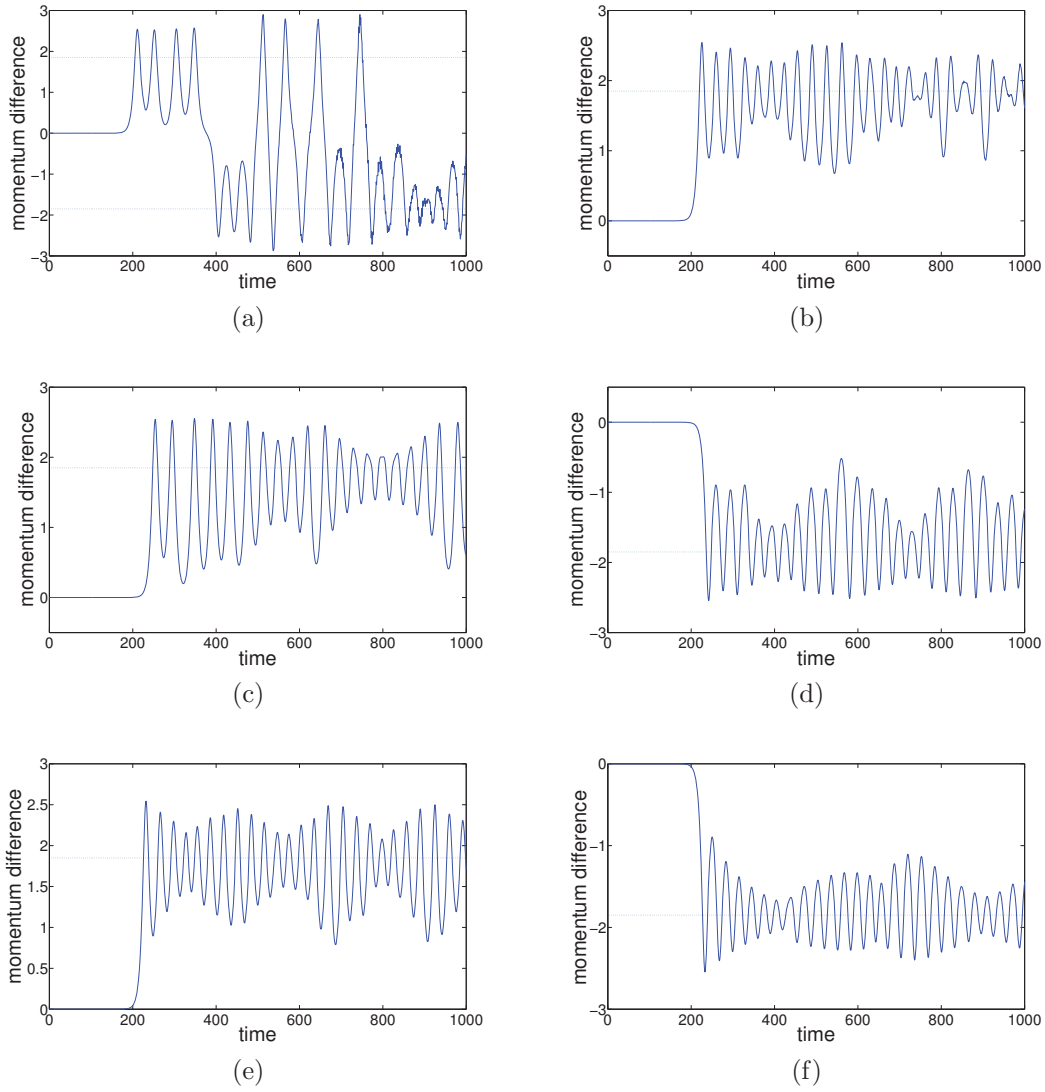

Figure 2.9: The momentum difference as a function of time, starting with a dark soliton for different box sizes L and tolerances of ode45 (low: rel.tol:10^{-3}, abs.tol:10^{-6}; high: rel.tol:10^{-10}, abs.tol:10^{-12}). The dotted line shows the location of the vortex ($\nu = 1/3$). (a) $L = 10$, low (b) $L = 30$, low (c) $L = 10$, high (d) $L = 30$, high (e) $L = 60$, high (f) $L = 120$, high. From plots (e) & (f) one can see damping of the oscillations up to the time when the first phonons return.

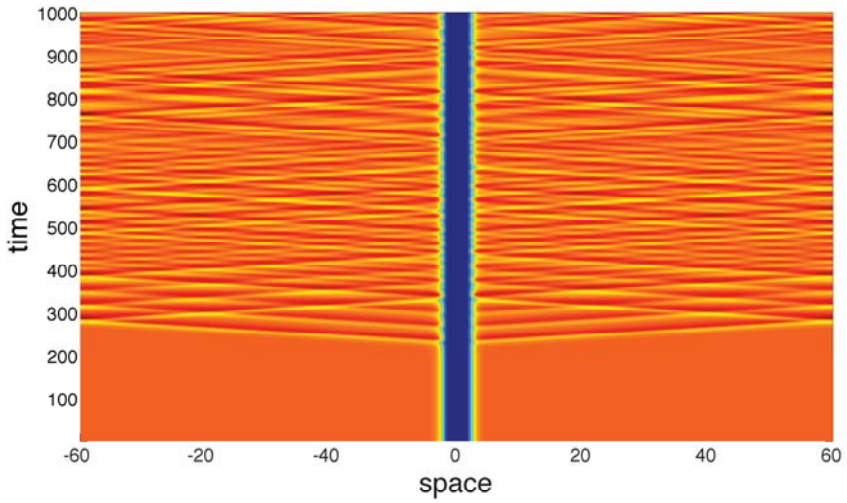

(a)

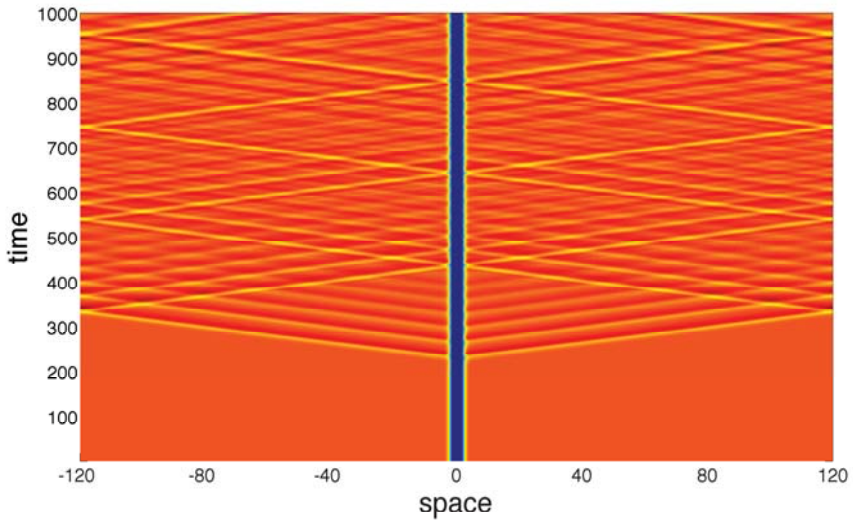

(b)

Figure 2.10: 'Density distribution' in the condensate during time propagation, ode45 rel.tol:10^{-10}, abs.tol:10^{-12}. Plotted is n^{30} to enhance the visibility of the phonon fringes. (a) L=60 (b) L=120.

the form

$$V(q) = \frac{m^\star \omega_a^2}{8a^2} \left(q^2 - a^2\right)^2 . \tag{2.26}$$

The parameter $m^\star$ corresponds to the effective mass, the variable q, given by the momentum difference ΔP, corresponds to "distance" in a classical picture,

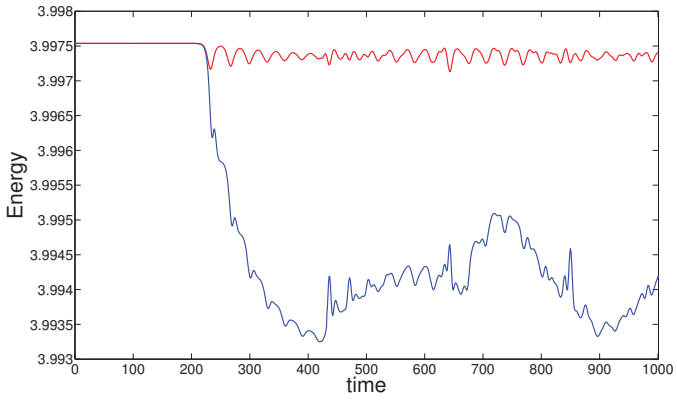

Figure 2.11: Total energy of the system (red line) and local energy in the area $[58, 62]$ of the soliton (blue line). $L = 120$, $\nu = 0.31$, ode45 rel.tol:10^{-10}, abs.tol:10^{-12}.

and the frequency ω_a can be interpreted as the curvature of the potential at the minima $q = \pm a$. Our potential has to fulfil the following requirements:

1. The height of the potential is determined by the energy difference of the (anti-)vortex and soliton. It can be calculated using equations (2.5) and (2.6).

2. The parameter a is given by the value of ΔP of the vortex. Its dependence on ν is shown in figure 2.8.

3. The curvature of the potential at $q = 0$ is expected to be harmonic, with a frequency ω_0 given by the imaginary eigenvalue of the Bogoliubov spectrum of the soliton.

4. Expanding the potential (2.26) in a Taylor series around the points $\pm a$ and 0 up to second order gives

$$V(\pm a + \epsilon) = \frac{1}{2} m^\star \omega_a^2 \epsilon^2, \tag{2.27}$$

$$V(\epsilon) = \frac{m^\star \omega_a^2}{8} a^2 - \frac{1}{4} m^\star \omega_a^2 \epsilon^2 \tag{2.28}$$

   and reveals harmonic behaviour in the vicinity of these points.

5. Combining constraints 3 and 4 results in the following relation of the two frequencies

$$\omega_a = \sqrt{2}\omega_0. \tag{2.29}$$

6. The frequency ω_a should appear in the Bogoliubov spectrum of the vortex.

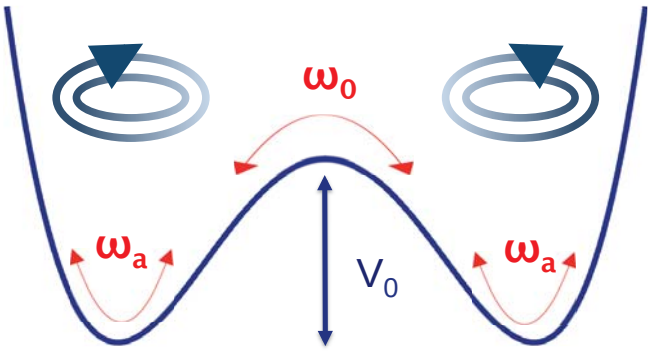

Figure 2.12: Scheme of the double well potential of equation (2.26).

Because the potential of equation (2.26) is somehow a wild guess, we undertake a few investigations to prove its validity. First of all we check the harmonic behaviour in the vicinity of the vortex and determine the frequency. Adding a dissipative term to parts of the time evolution serves the purpose of taking out additional energy and getting close to the vortex solution. It is introduced for technical reasons at this point and has no physical meaning here. The mixed time evolution reads

$$\mathrm{i}\partial_t \psi_j = (1 - \mathrm{i}\alpha)\left(-\frac{1}{2}\partial_{xx}\psi_j + |\psi_j|^2 \psi_j - \psi_j - \nu\psi_{3-j}\right). \tag{2.30}$$

The frequency can then be calculated from the period of oscillation τ via

$$\omega_a = 2\pi/\tau. \tag{2.31}$$

This procedure is shown in figure 2.13. While this process works well in the vicinity of the critical point $\nu = 0.31$, it can only be used as a rough estimate further away. The reason for that is the increasing energy difference between soliton and vortex state as one goes further away from the critical point (see figure 2.8). As can be seen from figure 2.10, phonons are emitted from the region of the density depression throughout the real time evolution and get reflected at the edges. In case of large ν the energy difference (and therefore the energy of the phonons) is small and the amplitude of harmonic oscillations is large. That makes it possible to take out the additional energy and simultaneously conserve the harmonic oscillations. For a smaller coupling constant the potential wells

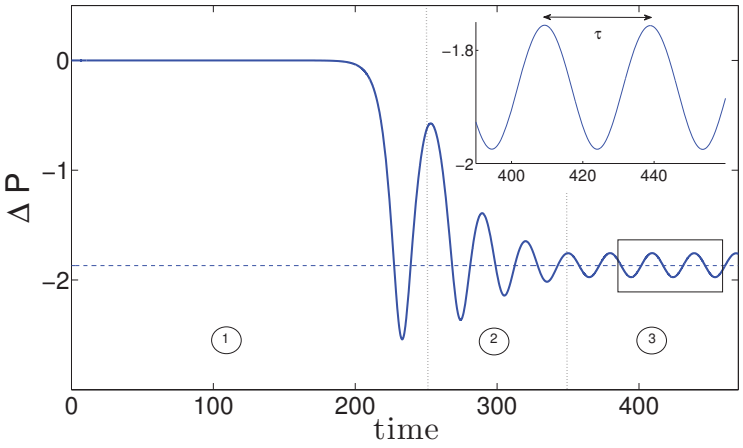

Figure 2.13: Time evolution of the soliton state (solid line) for $\nu = 0.31$. 1. Real time evolution shows the decay of a soliton into a vortex. 2. A damping term is switched on, taking out additional energy. 3. Real time evolution shows small harmonic oscillations around the vortex state. The dashed line gives the location of the vortex state. The frequency $\omega_a = 0.21$.

become narrower, resulting in smaller oscillation amplitudes. Simultaneously, the additional energy in the system increases. As a result we cannot avoid the effect of emitted and reflected phonons completely, since further damping reduces the amplitude of the harmonic oscillations as well. That means, when applying equation (2.30) to the regime of small ν we end up with a superposition of several oscillations. We relate the main frequency to the frequency of small oscillations around the vortex and identify the envelope with the return-time of phonons reflected from the boundaries of the computational box. For a system with $L = 60$ the traveling time of phonons from the location of the vortex and back, can be read off figure 2.10a and is approximately $t = 125$. This value matches with the frequency of the harmonic oscillation of the envelope in figure 2.14 showing the result for $\nu = 0.1$.

From table 2.3 we deduce the validity of the potential with respect to the constraint of equation (2.29). Although this relation is not perfectly fulfilled, it shows a sufficient agreement to hold on to the potential of equation (2.26).

A further supporting hint is the appearance of the frequency ω_a in the Bogoliubov spectrum of the vortex in the vicinity of the critical point $\nu = 1/3$. Further away from the critical point the frequency ω_a is not determined adequately enough to allow for this statement.

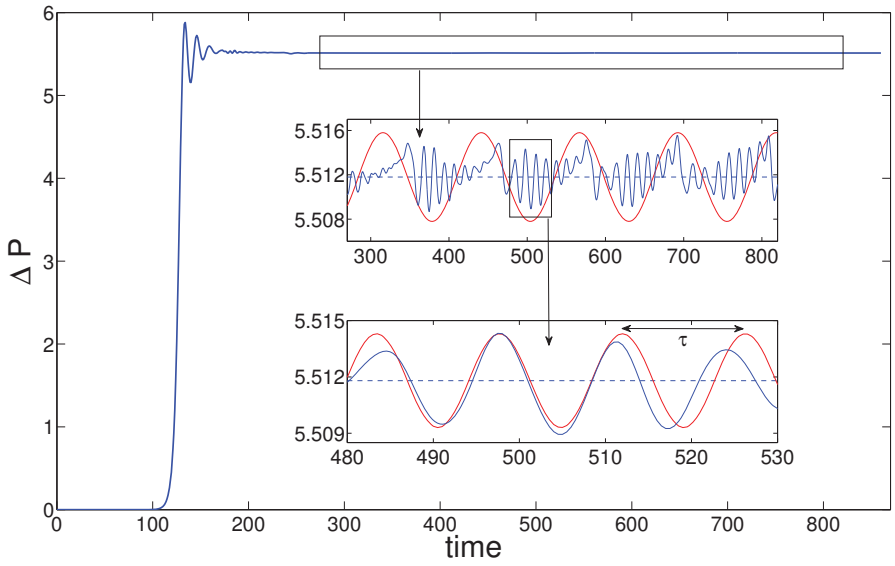

Figure 2.14: Mixed time evolution of the soliton state (solid line) for $\nu = 0.1$. The system size $L = [-60, 60]$, $\alpha = 0.04$. The times for real - mixed - real time propagation are $t_1 = 130$, $t_2 = 130$, $t_3 = 600$. The dashed line in the subplots gives the location of the vortex state. The frequency is found to be $\omega_a = 0.44$.

ν	τ	ω_a	$\tilde{\omega}_0$	ω_0	V_0	a	$m^\star$	E_0	E_1
0.31	29.9	0.21	0.15	0.1522	0.0044	1.8777	0.2155	0.1189	0.4351
0.15	13.4	0.47	0.33	0.2994	0.3452	4.9941	0.6176	0.1803	0.2028
0.1	14.3	0.44	0.31	0.2771	0.6310	5.5118	1.0820	0.1872	0.1878
0.05	18.0	0.35	0.25	0.2174	1.1101	5.9355	2.6668	0.1509	0.1509

Table 2.3: Parameters of the double well potential for different values of the tunnel coupling ν. From mixed time propagation we obtain: the periodicity of harmonic oscillations in the vicinity of the vortex τ, the corresponding frequency $\omega_a = 2\pi/\tau$ and $\tilde{\omega}_0 = \omega_a/\sqrt{2}$. From analytics we obtain: the curvature at the location of the soliton ω_0 obtained from the Bogoliubov spectrum (see fig 2.6a), the potential height V_0 (equation 2.35), the position of the vortex a (equation 2.25), the effective mass of the vortex $m^\star = 4V_0/\omega_0^2 a^2$, the zero point energy E_0 and the energy of the first excited state E_1 (eigenvalues of the Hamiltonian of equation 2.36). The simulation parameters are $L = 60$, $\alpha = 0.4$.

All investigations so far describe a classical particle in a double well potential, but with the aim of studying quantum tunnelling through the barrier we need to take quantum properties into account. In quantum mechanics the energy levels are quantised and the two lowest provide information about the tunnelling time. In a first approach we might approximate the two wells by a purely harmonic potential. In that case the zero point energy reads

$$E_g = \frac{\omega_a}{2} = \frac{\omega_0}{\sqrt{2}}, \tag{2.32}$$

and the tunnelling time can be estimated via the WKB method (see section 2.6). In order to obtain a more accurate estimate of tunnelling times we want to take a closer look at the exact energy levels in the double well potential of equation (2.26). Substituting the effective mass

$$m^\star = 4V_0/\omega_0^2 a^2, \tag{2.33}$$

in equation (2.26), the effective potential can be written in the form

$$V(q) = \frac{V_0}{a^4}\left(q^2 - a^2\right)^2, \tag{2.34}$$

where V_0 is the energy difference between the soliton and the vortex. It can be calculated using equations (2.5) and (2.6) to give

$$V_0 = \frac{8}{3}\left(\sqrt{\nu}(3-\nu) - (1+\nu)^{3/2}\right). \tag{2.35}$$

The parameter a is given by the positive sign solution of expression (2.25). The energies are now given by the eigenvalues of the Hamiltonian

$$H = -\frac{1}{2m^\star}\partial_{qq} + \frac{V_0}{a^4}\left(q^2 - a^2\right)^2. \tag{2.36}$$

We solve the problem numerically using the exact expressions for $m^\star$ and V_0, and a five point stencil for the second derivative. A comparison of the two lowest levels with the height of the potential is shown in figure 2.15. We find the upper/lower energy level performing a crossover with the potential at a value around $\nu = 0.18/\nu = 0.22$. Below these values we expect quantum tunnelling from the vortex to the antivortex. In case the two energy levels exceed the

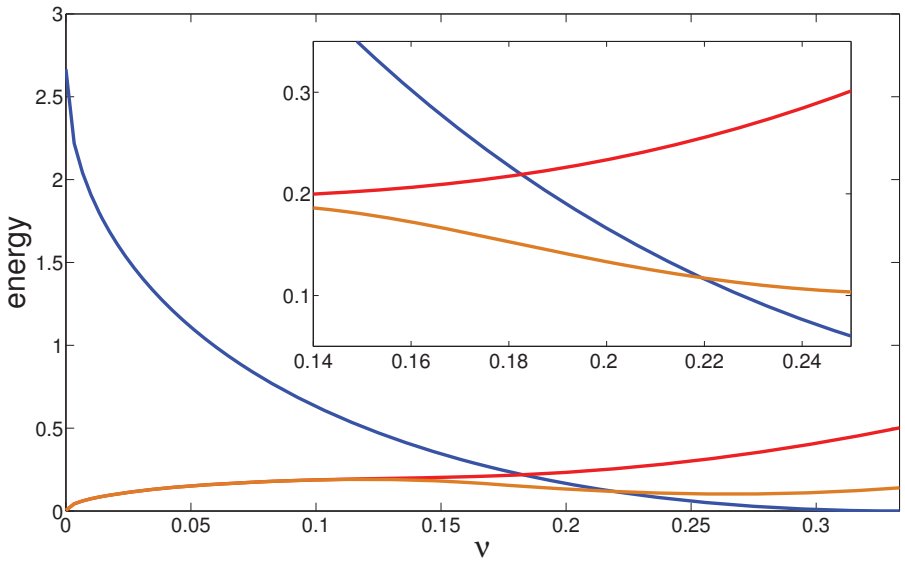

Figure 2.15: Energies of the double well potential. The potential barrier V_0 of the double well potential of equation (2.34) is given by the blue line. The ground state energy E_0 and first excited state energy E_1 of the double well potential obtained by solving equation (2.36) are given by the orange and red line respectively.

potential barrier one can still look for a vortex/antivortex transition, although no tunnelling is involved here. Figure 2.16 shows the comparison of the harmonic potential ground state energy of equation (2.32) with the exact values. We find them matching in a regime of low tunnel coupling up to about $\nu < 0.1$. In this regime we expect the WKB method to give accurate results for the tunnelling time (see section 2.6). The energies E_0, E_1 together with the potential height V_0 are listed in table 2.3. The expected frequency of vortex - antivortex oscillations is given by

$$\Omega = (E_1 - E_0)/2, \tag{2.37}$$

which is shown in figure 2.17 as a function of ν. In figure 2.18 we sketch the energy levels in the double well potential together with the corresponding wave functions. Figure 2.19 shows the probability density of the symmetric/antisymmetric combination of the two eigenstates which locate the system at the position of the vortex/antivortex.

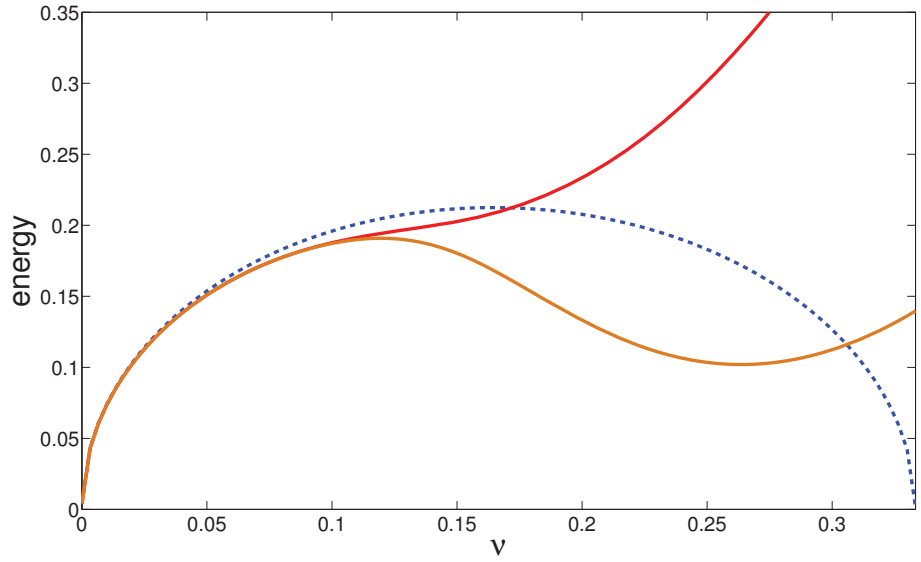

Figure 2.16: Comparison of the actual ground/first excited state energies E_0/E_1 (orange/red line) of the Hamiltonian of equation (2.36) with the harmonic approximation $E_g = \omega_0/\sqrt{2}$ (dotted blue line), as a function of the tunnel coupling. A strong deviation shows for $\nu > 0.1$.

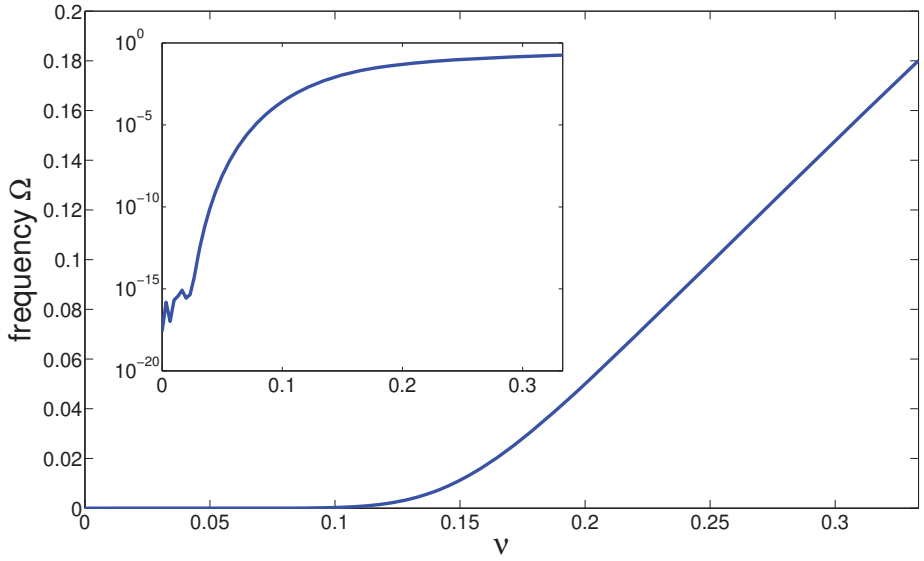

Figure 2.17: The expected frequency of vortex-antivortex oscillation given by equation (2.37) as a function of the tunnel coupling ν. Calculations are based on the double well potential of equation (2.34). The inset shows the same data on a logarithmic scale. For $\nu < 0.026$ numerical accuracy limits a precise statement.

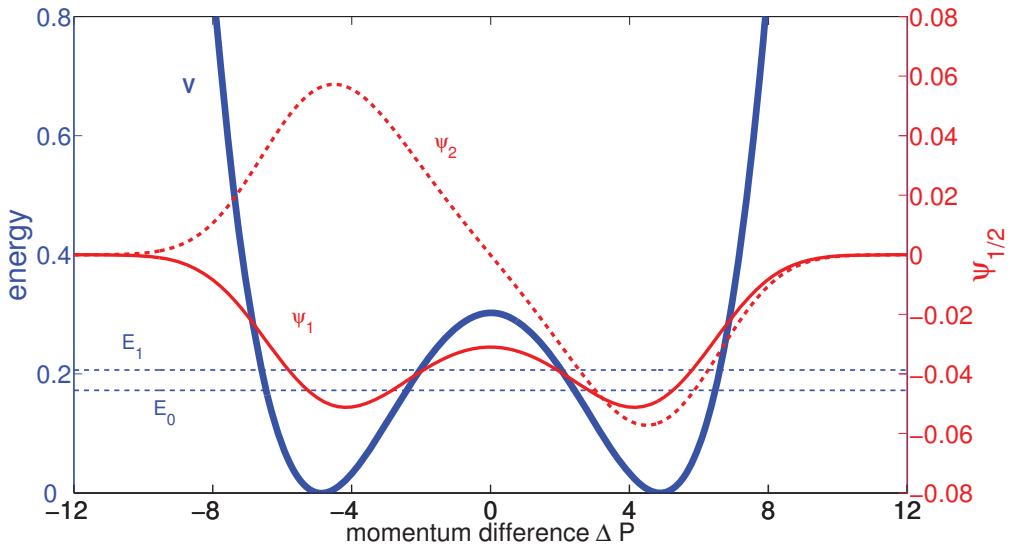

Figure 2.18: Sketch of the double well potential of equation (2.34) (blue line) together with its ground- and first excited state energies E_0/E_1 (dotted blue lines) and the corresponding wave functions (full/dotted red line). The energies and wave functions are obtained from the Hamiltonian of equation (2.36) using a fife point stencil for the second derivative and applying the Matlab routine 'eigs'. While the ground state is symmetric with respect to the soliton solution of $\Delta P = 0$, the first excited state is antisymmetric. Here, a tunnel coupling of $\nu = 0.16$ is used.

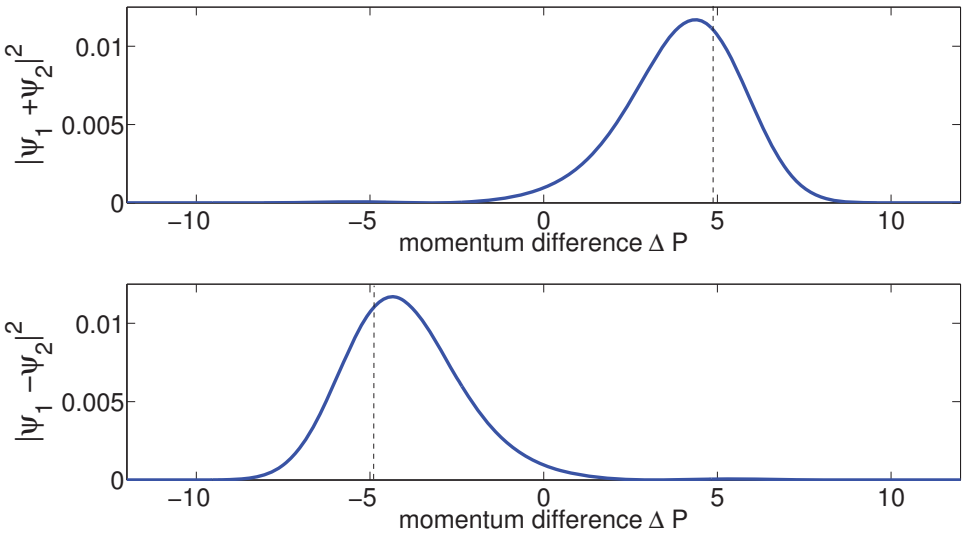

Figure 2.19: Probability density of the symmetric/antisymmetric combination of the two lowest eigenstates of the Hamiltonian of equation (2.36). We find the system localised around the vortex/antivortex state, which is indicated by the dashed line. To allow for comparison with figure 2.18 the tunnel coupling is set to $\nu = 0.16$.

2.6 Outlook

A very common method of calculating tunnelling times in a quasi-classical situation is known as WKB method. It approximates the energy splitting of the two lowest levels under the conditions of a slowly varying potential barrier. Since this method is based on a quasi-classical assumption, the energy of the states has to be sufficiently high to ensure classical motion. Comparing the WKB tunnelling times with the ones obtained in chapter 2.5 provides information about the semiclassical regime.

A more advanced way of studying quantum tunnelling is by the use of phase space techniques, such as the Wigner-, P- or positive-P method. Tunnelling is induced by quantum fluctuations which are explicitly included in the initial state as noise. Expectation values are obtained by sampling over many trajectories in phase space. As mentioned in the introduction, it is very important for each of these methods to choose the correct distribution of initial functions and therefore adequate noise modes. A reasonable choice is the elementary excitations spectrum (phonons) which we calculated in section 2.2 & 2.3 by solving

the Bogoliubov de-Gennes equations. This can now be used to implement e.g. the truncated Wigner method.

Another open question is, if or to what amount, the phonons suppress the vortex-antivortex tunnelling. The Caldeira-Leggett model [48] describes dissipation via coupling to a bath of harmonic oscillators, which is in the case of a two-level system known as Spin-Boson model. This might be a good way of treating our system. In order to avoid the unphysical reflections of phonons from the edges of the finite computational box, one might also think of introducing absorbing boundaries. This topic has been discussed in the context of non-linear Schrödinger equations in a variety of papers [49, 50, 51].

Chapter 3

Ground state calculation of annular BECs

In this chapter we propose a system consisting of two coupled, one-dimensional Bose-Einstein condensates as a promising candidate for the study of macroscopic quantum tunnelling of vortices. For a single ring we find the angular momentum of the ground state of the rotating system dependent on the radius of the trap. In a coupled system of two rings with different radii two effects determine the behaviour of the ground state: the tunnel coupling prefers to align the phases in the two rings, while rotation in general prefers different phases. As a compromise the phase difference is accumulated over a small area, resulting in the occurrence of vortices. We show that vortices can be pinned by external potentials. Raising a second potential may lead to tunnelling of the vortex from one potential to the other. Most of the performed calculations are similar to an earlier work of Brand *et al.* [52]. We review them using the program package Xmds2 for the numerics concerning partial differential equations.

3.1 Single annular Bose-Einstein condensate

We start with determining the ground state properties of a single rotating annular condensate. We are particularly interested in the radius dependence of the solution. The system is sketched in figure 3.1. Because of the rotational symmetry it is convenient to choose the angle θ as our parameter. We account for the rotation by switching to the rotating frame of reference. Although the

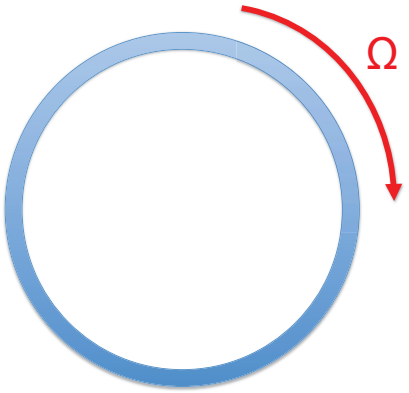

Figure 3.1: Sketch of a one-dimensional annular condensate rotating with trap frequency Ω.

Hamiltonian does not contain a corresponding term explicitly, we assume an equilibrating process to be present, e.g. irregularities in the trap geometry, which allows the system to evolve to its ground state in the rotating frame. The new absolute energy minimum is shifted to a state rotating at a frequency close to the one of the trap. The equation of motion in the rotating frame is obtained by adding the term $-\Omega L_z$ to the Hamiltonian, where Ω is the angular velocity of the trap and $L_z = -\mathrm{i}\hbar\partial_\theta$ the angular momentum operator. The Gross-Pitaevskii equation therefore acquires an extra term and, in dimensionless units (see appendix B), reads

$$\mathrm{i}\partial_t\psi(\theta,t) = -\frac{1}{2R^2}\partial_{\theta\theta}\psi(\theta,t) + |\psi(\theta,t)|^2\,\psi(\theta,t) - \psi(\theta,t) + \mathrm{i}\Omega\partial_\theta\psi(\theta,t), \quad (3.1)$$

R denoting the radius of the trap. The ground state of a condensate in a resting trap is a stationary solution with constant density. It is known, that the condensate in a rotating trap moves with the trap at a frequency as close as possible to the trap frequency Ω. Since the phase, which determines the velocity of the condensate (see section 1.2.1), has to be a continuous function, the phase difference over the condensate is always a multiple of 2π. Therefore, the frequency of the condensate cannot always match the frequency of the trap.

We calculate the ground state of the rotating system using imaginary time evolution. The idea of this procedure is explained in appendix A.1. After substituting $t \to \tau = \mathrm{i}t$, the Gross-Pitaevskii equation (3.2) in imaginary time reads

$$\partial_\tau\psi(\theta,\tau) = \frac{1}{2R^2}\partial_{\theta\theta}\psi(\theta,\tau) - |\psi(\theta,\tau)|^2\,\psi(\theta,\tau) + \psi(\theta,\tau) - \mathrm{i}\Omega\partial_\theta\psi(\theta,\tau). \quad (3.2)$$

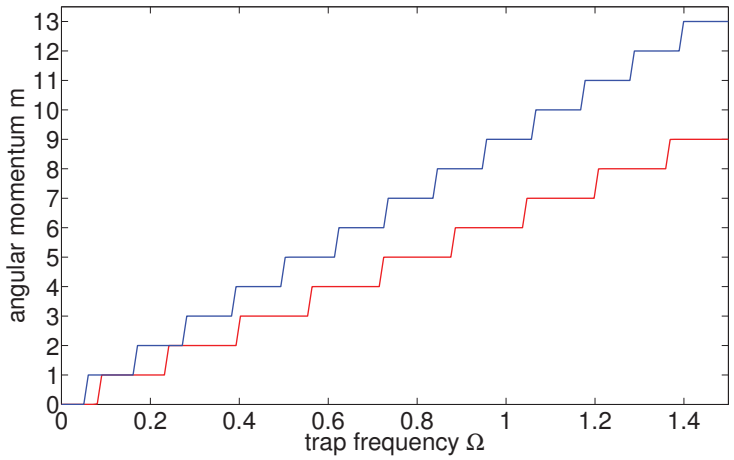

Figure 3.2: The angular momentum of the ground state of an annular condensate depends on the trap frequency as well as on the radius of the ring. The red line corresponds to $R = 2.5$, the blue one to $R = 3$. The propagation time is $t = 100$.

As the initial state we take a linear combination of plane waves that is normalised to $\int |\psi|^2 \, d\theta = 2\pi$. Since the procedure of imaginary time propagation does not conserve the norm, we normalise the wave function after each time step. After propagating the system to the ground state, we calculate the angular momentum of the condensate. It reads in dimensionless units (see appendix B)

$$\langle L \rangle = -\frac{\mathrm{i}}{2\pi} \int \psi^* \partial_\theta \psi d\theta. \tag{3.3}$$

As expected, the angular momentum plotted against the trap frequency is a step function. From figure 3.2 we see that the angular momentum depends on the trap radius.

3.2 Coupled annular Bose-Einstein condensates

We now investigate properties of the ground state of two coupled one-dimensional annular Bose-Einstein condensates, rotating at a trap frequency Ω. In general the two rings have different radii, which is sketched in figure 3.4. As can be seen from figure 3.2, at a given trap frequency, the condensate in the outer ring will favour a higher angular momentum than the one in the inner ring. Since

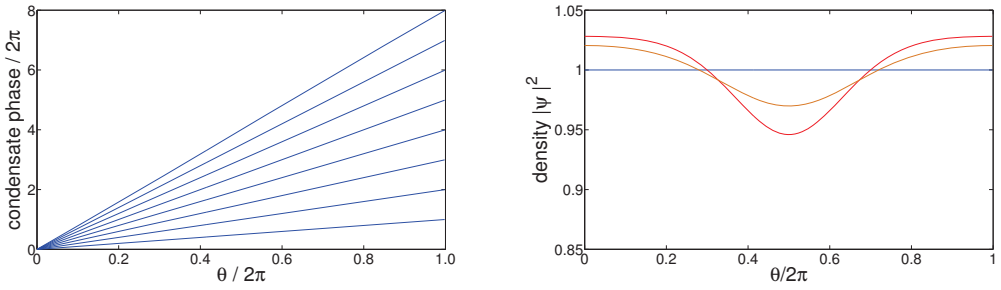

(a) (b)

Figure 3.3: (a) The phase of the condensate wave function for a single ring of radius $R = 2.5$ and trap frequencies $\Omega = [0, 0.15, 0.3, 0.45, 0.6, 0.75, 0.9, 1.05, 1.2, 1.35]$. (b) The density of the condensate wave function for $\Omega = [0, 0.2, 0.4, 0.6, 0.8, 1, 1.2, 1.4]$ after imaginary time propagation. The ground state density reaches a constant value (blue line). Longer propagation times are needed in the vicinity of a saltus of the angular momentum (see figure 3.2). Here the wave function at $t = 43$ for $\Omega = 0.4$ (red line) and $\Omega = 1.2$ (orange line) has not yet converged.

the two rings are linked via tunnelling they cannot evolve independently from each other. The effect of the coupling is to seek alignment of the phases. As a compromise of these two ambitions, the ground state appears to have the same phase for the two rings almost everywhere, except for some areas where a phase difference of 2π is accumulated. Since a phase difference indicates a flow in the system we associate these spots with a circular flow going over the tunnel barrier region. The core of this vortex is located in the middle of the tunnel barrier region between the two condensates. The number of vortices depends on the difference in angular momentum of the two uncoupled rings (see figure

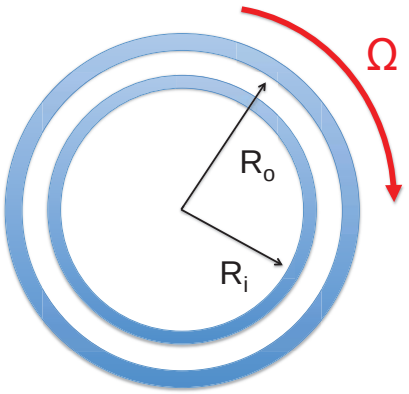

Figure 3.4: Sketch of coupled one-dimensional annular condensates rotating with trap frequency Ω.

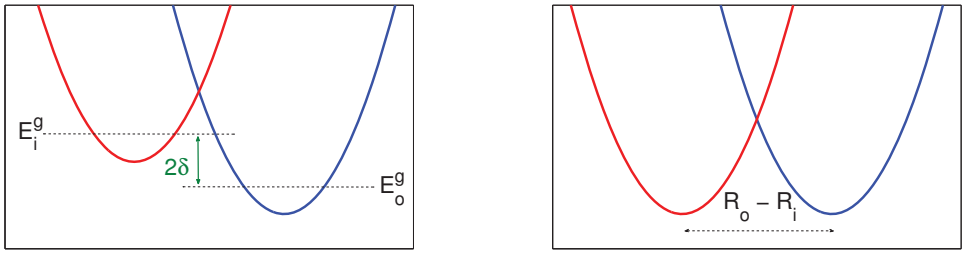

(a) (b)

Figure 3.5: Schematic illustration of the parabolic potential across the two rings. (a) Tilted configuration without external potential ($\delta = 0.$) (b) The external potential δ restores the symmetry.

3.2), as well as the magnitude of the tunnel coupling.

The Gross-Pitaevskii equations in dimensionless units (see appendix B) for the inner and outer ring wave functions ψ_i, ψ_o read

$$\mathrm{i}\partial_t\psi_i = -\frac{1}{2R_i^2}\partial_{\theta\theta}\psi_i + |\psi_i|^2\psi_i - \psi_i - \delta\psi_i + \mathrm{i}\Omega\partial_\theta\psi_i - \nu\psi_o \tag{3.4}$$

$$\mathrm{i}\partial_t\psi_o = -\frac{1}{2R_o^2}\partial_{\theta\theta}\psi_o + |\psi_o|^2\psi_o - \psi_o + \delta\psi_o + \mathrm{i}\Omega\partial_\theta\psi_o - \nu\psi_i. \tag{3.5}$$

Here, ν is the tunnel coupling constant given in units of the chemical potential and δ is an external potential. The latter has the effect of lowering/raising the energy in the inner/outer ring. This can be used to counteract the centrifugal force which pushes the atoms into the outer ring. Ideally, the two effects compensate each other ensuring the same number of particles in the inner and outer ring. The effect of δ on the potential across the uncoupled rings, is shown in figure 3.5. In order to find an estimate for δ, we calculate the energy difference $\Delta E = E_o - E_i$ of the ground states of the inner and outer ring $\psi_{i/o} = \exp(\mathrm{i}\theta m_{i/o})$. That gives

$$\delta = \left|\frac{\Delta E}{2}\right| = \left|\frac{1}{4}\left(\frac{m_o^2}{R_o^2} - \frac{m_i^2}{R_i^2}\right) - \frac{\Omega}{2}(m_o - m_i)\right|, \tag{3.6}$$

with $m_{i/o}$ being the quantum number of the angular momentum of the uncoupled condensates, taking only integer values. According to reference [52] it can be calculated using

$$m_{i/o} = \mathrm{Int}[R_{i/o}^2\Omega + 1/2], \tag{3.7}$$

which, for larger values of $m_{i/o}$ can be approximated by $m_{i/o} \approx R_{i/o}^2 \Omega$, allowing to write the energy difference as

$$\delta = \frac{\Omega^2}{4} \left(R_o^2 - R_i^2 \right). \tag{3.8}$$

Again, we calculate the ground state by propagating in imaginary time. In order to end up with a vortex in the ground state, one has to find a proper value for the tunnel coupling ν. A larger tunnel coupling constant favours the alignment of the phases repressing vortices. For the parameters used in figure 3.6a a single fluxon appears. Here, the outer ring favours $m_o = 5$ and the inner ring $m_i = 4$ which can be seen from figure 3.2 or calculated using equation (3.7).

The number of fluxons in the ground state can take any integer value between zero and $m_o - m_i$, depending on the tunnel coupling constant. The number of fluxons can be reduced by raising ν. Figure 3.7 shows solutions for different tunnel coupling constants but otherwise same parameters.

3.3 Pinning of vortices

In this section we investigate the influence of additional external potentials on the condensate wave function of two coupled annular Bose-Einstein condensates. In the case of a repulsive potential the particles try to avoid this region in order to minimise the energy. A vortex always shows a density dip in both rings and therefore it is energetically favourable for the system to shift the centre of the vortex to the position of the potential. As a results we find the possibility of pinning vortices by repulsive external potentials.

3.3.1 The double well potential

We start with a configuration of a single vortex in the ground state, which we find by evolving in imaginary time. This initial configuration is shown in figure 3.8a. Then slowly, we raise a potential on one side of the vortex. After a time T_V the potential remains at its maximum value. During all steps we continue with the imaginary time propagation. The differential equations in imaginary

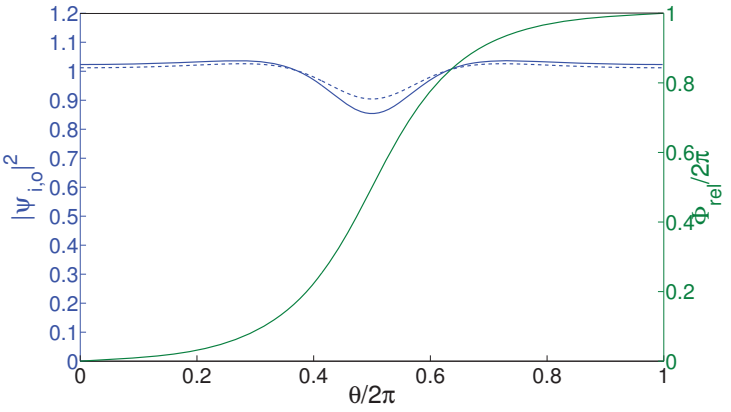

(a)

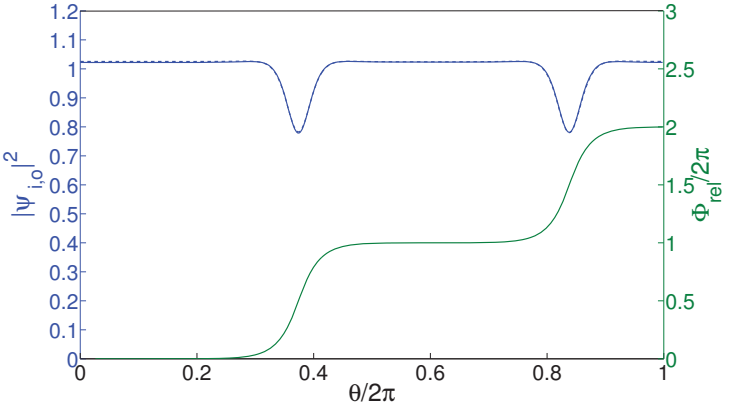

(b)

Figure 3.6: The ground state of the rotating, coupled, annular system showing fluxons. The density of the inner/outer ring is given by the blue dashed/full line. The green line gives the relative phase between the two condensates. The parameters are (a) $R_o = 3$, $R_i = 2.5$, $\nu = 0.08$, $\delta = 0.23$, $\Omega = 0.58$(b) $R_o = 11$, $R_i = 10.5$, $\nu = 0.08$, $\delta = 0.107$, $\Omega = 0.2$.

time τ read

$$\begin{aligned}\partial_\tau \psi_{i/o} = \frac{1}{2R_{i/o}^2}\partial_{\theta\theta}\psi_{i/o} - \left|\psi_{i/o}\right|^2\psi_{i/o} + (1 \pm \delta)\psi_{i/o} - \mathrm{i}\Omega\partial_\theta\psi_{i/o} \\ -f(\tau)V_{\mathrm{ext}}\psi_{i/o} + \nu\psi_{o/i},\end{aligned} \tag{3.9}$$

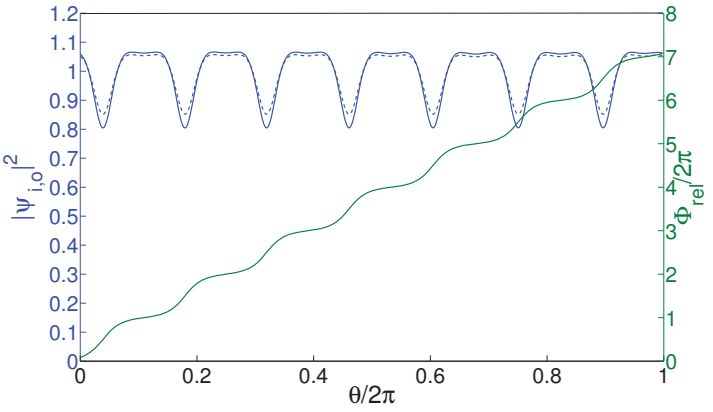

(a)

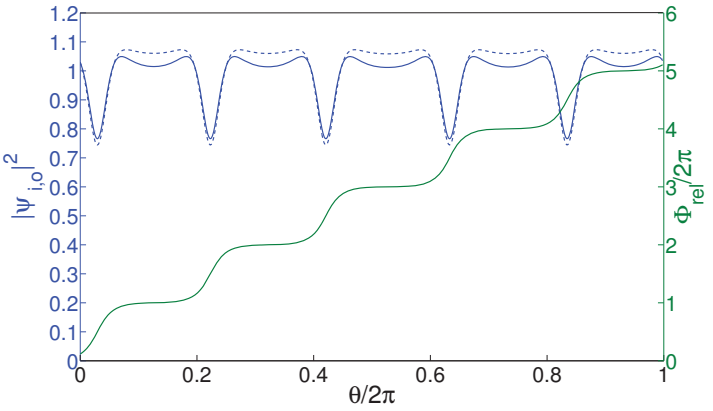

(b)

Figure 3.7: The ground state of the rotating, coupled, annular system for different values of the tunnel coupling constant. The density of the inner/outer ring is given by the blue dashed/full line. The green line gives the relative phase between the two condensates. The parameters are $R_o = 11$, $R_i = 10$, $\delta = 0.84$, $\Omega = 0.4$ (a) $\nu = 0.140$ (b) $\nu = 0.18$.

where the function $f(\tau)$ is given by

$$f(\tau) = \begin{cases} \tau/T_{\mathrm{V}} & \text{if} \quad \tau \leq T_{\mathrm{V}} \\ 1 & \text{if} \quad \tau > T_{\mathrm{V}} \end{cases} \tag{3.10}$$

The increase of the potential is performed adiabatically, meaning the system has enough time to adjust to the new situation and never makes it far from the

ground state. We choose a Gauss distribution for the potential of the form

$$V_{\text{ext}}(\theta) = Ae^{-\frac{1}{2}(\frac{\theta-\theta_0}{\sigma})^2}, \tag{3.11}$$

where A is the maximum peak value, σ the width and θ_0 the peak position of the potential. Raising the repulsive potential creates a dip in the density of the wave function which attracts the vortex in case it is close enough. Figure 3.8b shows the result where the vortex ends up at the location of the external potential.

We now want to investigate the behaviour of a vortex under the influence of two pinning potentials. The external potential takes the form

$$V_{\text{ext}}(\theta) = A\left(e^{-\frac{1}{2}(\frac{\theta-\theta_0}{\sigma})^2} + e^{-\frac{1}{2}(\frac{\theta-\theta_0'}{\sigma})^2}\right). \tag{3.12}$$

We choose the peak positions θ_0 and θ_0' such that the vortex is initially located in between the two potentials. For large separation we find the vortex attracted by the potential closer to it. Figure 3.9 shows the ground state of the system with the fluxon pinned by one of the external potentials. The initial configuration coincides with the one given in figure 3.8a. When the distance undercuts a certain value, the vortex stays pinned in the middle. That happens at the point where the two Gauss functions start to overlap. A similar behaviour of a vortex in a 2D Bose gas was found by Fialko *et al.* [3]. Figure 3.10 shows the position of the vortex as a function of the separation of the external potentials. From these calculations one can estimate the minimum separation of the two potentials for which quantum tunnelling is possible.

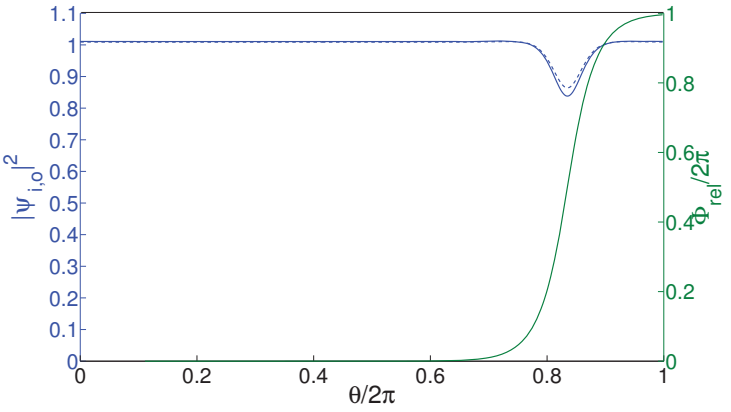

(a)

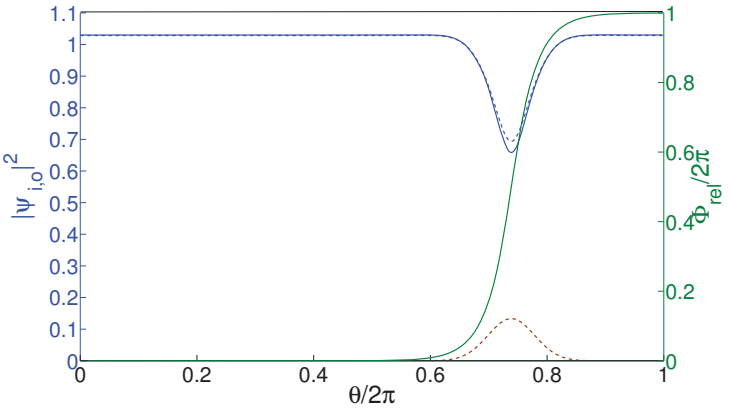

(b)

Figure 3.8: (a) Ground state of two coupled annular condensates with the parameters $R_o = 11$, $R_i = 10.5$, $\delta = 0.0605$, $\Omega = 0.15$, $\nu = 0.05$. (b) Ground state under the influence of an external potential with the parameters $\sigma = 0.25$, $A = 0.2$. The blue full/dotted line is the density of the outer/inner ring, the green line is the phase difference of the inner and outer wave function and the dotted brown line shows the position of the external potential.

3.4 Outlook

A vortex pinned by external potentials is a promising candidate for the detection of macroscopic quantum tunnelling. As already mentioned in section 2.6, tunnelling times can be estimated using the semiclassical WKB method. For that one will have to write down the effective potential separating the two degenerate states where the vortex is pinned by the left or right potential. The potential

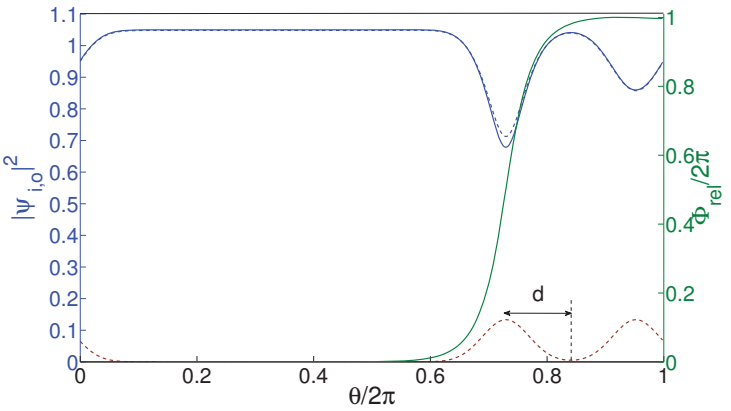

Figure 3.9: Ground state of two coupled annular condensates under the influence of two pinning potentials. The parameters of the trap are $R_i = 10.5$, $R_o = 11.0$, $\Omega = 0.15$, $\delta = 0.0605$, $\nu = 0.05$. The parameters of the pinning potentials are $\sigma = 0.25$, $A = 0.2$, $d = 0.7$.

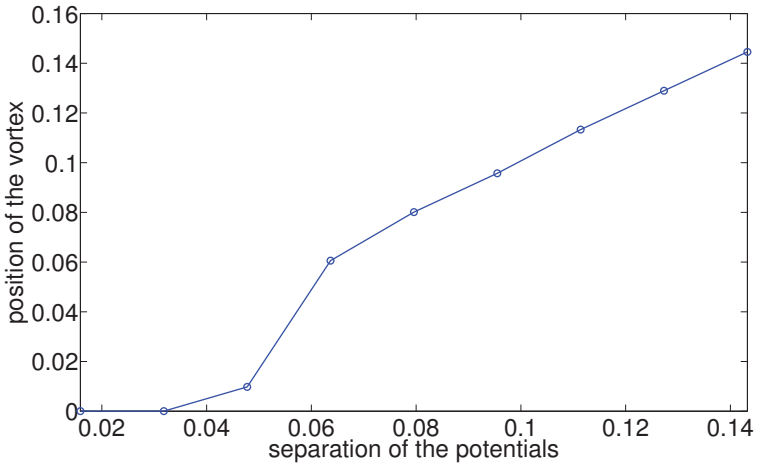

Figure 3.10: Displacement of the vortex from the centre between the two pinning potentials as a function of the separation d of the two external potentials in units of $\theta/2\pi$. The parameters of the trap are $R_i = 10.5$, $R_o = 11.0$, $\Omega = 0.15$, $\delta = 0.0605$, $\nu = 0.05$. The parameters of the pinning potentials are $\sigma = 0.25$, $A = 0.2$.

barrier can be adjusted by changing the amplitude of the external potentials or the distance of the two Gauss potentials (see figure 3.10). One might try an ansatz the form of equation (2.26) and undertake similar steps as in section 2.5 to validate it.
This should be compared to a truncated Wigner simulation, which includes quantum fluctuations triggering the transition.

Chapter 4

Conclusion

In this work we presented two different realisations of coupled one-dimensional Bose-Einstein condensates, which are both promising candidates for the study of macroscopic quantum tunnelling.
In case of the linear system, the two distinct macroscopic states are given by Josephson vortices, rotating in opposite directions. Starting with known analytic expressions for the soliton and the vortex, we calculated the corresponding Bogoliubov spectrum, finding the soliton to be unstable in a certain parameter regime of the tunnel coupling constant. An analytic result for the unstable eigenenergies and corresponding modes was presented. Propagating the soliton in real time showed the decay into a vortex. We presented a very simple form of the effective potential the vortex experiences and calculated the regime where quantum tunnelling can be detected. This, together with the Bogoliubov spectrum allows for future studies using the semiclassical WKB method or the numerical truncated Wigner method.

The second configuration consists of two ring shaped condensates, where vortices appear in the ground state of the rotating system. We revisited the radius dependence of the angular momentum of a single ring, as well as the conditions for the parameters in order to end up with a certain number of vortices. It was found that a repulsive external potential attracts and pins the vortex. We proposed a configuration of two external potentials as a promising system to study macroscopic quantum tunnelling.

Appendix A

Methods calculating stationary solutions

A.1 The imaginary time propagation method (ITP)

The ITP method is a tool to approximate the ground state wave function to arbitrary accuracy. One substitutes the real time in the time-dependent Schrödinger equation with imaginary time, which leads to an exponential decay of all components but the ground state. In order to explain the idea of this method we write down the time-dependent Schrödinger equation and start with an arbitrary guess for the wave function $\psi(t)$

$$\mathrm{i}\hbar\frac{\partial}{\partial t}\psi(t) = H\psi(t). \tag{A.1}$$

Rewriting this equation into imaginary time reads

$$\frac{\partial}{\partial \tau}\psi(\tau) = -H\psi(\tau), \qquad \tau = \mathrm{i}t/\hbar. \tag{A.2}$$

The wave function ψ can be written as a sum of eigenfunctions of the Hamiltonian $\psi(\tau) = \sum_i c_i\psi_i(\tau)$. For each component the solution to equation (A.1) is an exponent of the form $\psi_i(\tau) = \mathrm{e}^{-E_i\tau}\psi_i(0)$, and for the total wave function

we get

$$\psi(\tau) = \sum_i c_i \mathrm{e}^{-E_i \tau} \psi_i(0). \tag{A.3}$$

Thus, all scattering components will vanish exponentially, while all bound states grow exponentially in time. For sufficient long propagation time τ we find only the lowest energy state surviving - all others dying out. The probability of finding the system in the ground state reaches 1 for infinite time because $E_i > E_0$

$$\lim_{\tau\to\infty} \frac{\langle\psi(\tau)|c_0\psi_0(\tau)\rangle}{\langle\psi(\tau)|\psi(\tau)\rangle} = \frac{c_0^2 \mathrm{e}^{-2\tau E_0}}{c_0^2 \mathrm{e}^{-2\tau E_0} + \sum_{i=1}^{\infty} c_i^2 \mathrm{e}^{-2\tau E_i}} = 1. \tag{A.4}$$

The only constraint to this procedure is, that the initial wave functions needs to contain a non-zero component of the ground state.

In the case of the non-linear GPE, the energy of the system depends on the norm $|\psi|^2$. Since the imaginary time propagation doesn't conserve the norm a priori, the wave function has to be renormalised during the procedure. Alternatively one might introduce a chemical potential which fixes the number of particles in the system.

A.2 Broyden's method

Broyden's method [53] is a generalisation of the Newton-Raphson method which allows us to calculate the roots of a system of equations in an iterative way. The idea behind this method becomes clear for a single function. Starting with an initial guess, which is reasonable close to the real root, one calculates the derivative at this point to find a better approximation using

$$x_{n+1} = x_n - \frac{f(x_n)}{f'(x_n)}. \tag{A.5}$$

This procedure is repeated until the difference in the solution reaches a critical value. For a system of equations $F(x) = 0$, the derivative in equation (A.5) is replaced by the Jacobian matrix J, reading

$$x_{n+1} = x_n - J_n^{-1} F(x_n). \tag{A.6}$$

Since the Jacobian is highly expensive to calculate, Broyden suggested to calculate the Jacobian only once and take an estimate for all following steps using

$$J_n = J_{n-1} + \frac{\Delta F_n - J_{n-1}\Delta x_n}{|\Delta x_n|^2}\Delta x_n^T. \tag{A.7}$$

The inverse of the Jacobian, needed to evaluate equation (A.6), can be calculated using

$$J_n^{-1} = J_{n-1}^{-1} + \frac{\Delta x_n - J_{n-1}^{-1}\Delta F_n}{\Delta x_n^{\mathrm{T}} J_{n-1}^{-1}\Delta F_n}\left(\Delta x_n^{\mathrm{T}} J_{n-1}^{-1}\right). \tag{A.8}$$

The main advantage of Broyden's method compared to imaginary time propagation is the ability to find all roots to the equations - not only the lowest energy state. That allows us to look for local minima, maxima and saddle points.

Appendix B

Dimensionless units

For simplicity we write our equations in dimensionless units. In this section we review the reference parameters for the quantities used.

B.1 The Gross-Pitaevskii equation in dimensionless units

Following the example of Kaurov&Kuklov [25] we write the Gross-Pitaevskii equation in a convenient dimensionless form. Starting from the original version

$$\mathrm{i}\hbar\partial_t\psi(x,t) = -\frac{\hbar^2}{2m}\partial_{xx}\psi(x,t) + g\left|\psi(x,t)\right|^2\psi(x,t) - \mu\psi(x,t) \tag{B.1}$$

we renormalise the parameters: order parameter $\tilde{\psi} = \psi/\sqrt{n_0}$, spatial coordinate $\tilde{x} = x/x_0$ and time $\tilde{t} = t/t_0$, with n_0 being the background density of the one-dimensional system. Substituting that into equation (B.1) and dividing by μ, we get

$$\mathrm{i}\frac{\hbar}{t_0\mu}\partial_{\tilde{t}}\tilde{\psi}(\tilde{x},\tilde{t}) = -\frac{\hbar^2}{2m\mu x_0^2}\partial_{\tilde{x}\tilde{x}}\tilde{\psi}(\tilde{x},\tilde{t}) + \frac{gn_0}{\mu}\left|\tilde{\psi}(\tilde{x},\tilde{t})\right|^2\tilde{\psi}(\tilde{x},\tilde{t}) - \tilde{\psi}(\tilde{x},\tilde{t}). \tag{B.2}$$

Because the chemical potential can be written in the form $\mu = gn_0$, the factor in front of the non-linear term always takes the value of 1. Using the general

expression for the healing length ξ

$$\xi = \sqrt{\frac{\hbar^2}{2m\mu}} \tag{B.3}$$

we define our units in terms of the healing length and the chemical potential as

$$x_0 = \sqrt{\frac{\hbar^2}{m\mu}} = \sqrt{2}\xi \tag{B.4}$$

$$t_0 = \frac{\hbar}{\mu} = \frac{2\xi^2 m}{\hbar}. \tag{B.5}$$

Energy is therefore measured in units of μ. Substituting $\tilde{t} \to t$, $\tilde{x} \to x$ and $\tilde{\psi}(\tilde{x}, \tilde{t}) \to \psi(x, t)$, the dimensionless Gross-Pitaevskii equation reads

$$\mathrm{i}\partial_t \psi(x,t) = -\frac{1}{2}\partial_{xx}\psi(x,t) + |\psi(x,t)|^2 \psi(x,t) - \psi(x,t). \tag{B.6}$$

The non-linear coupling and the chemical potential always take the value of 1. The number of particles in the system is given by

$$N = x_0 n_0 \int |\psi|^2 \, dx. \tag{B.7}$$

Rotation term

We account for rotation by adding the term

$$\mathrm{i}\hbar\Omega\partial_\theta\psi(x,t) \tag{B.8}$$

to the equation of motion (B.1). Renormalising as above and dividing by μ, we get

$$\frac{\mathrm{i}\hbar}{\mu}\Omega\partial_\theta\tilde{\psi}(\tilde{x},\tilde{t}) = \mathrm{i}t_0\Omega\partial_\theta\tilde{\psi}(\tilde{x},\tilde{t}). \tag{B.9}$$

Renormalising the frequency by $\tilde{\Omega} = \Omega/\Omega_0 = t_0\Omega$ and substituting back $\tilde{\psi}(\tilde{x}, \tilde{t}) \to \psi(x, t)$, $\tilde{\Omega} \to \Omega$ we get

$$\mathrm{i}\Omega\partial_\theta\psi(x,t) \tag{B.10}$$

Therefore, frequency is measured in units of $\Omega_0 = 1/t_0 = \mu/\hbar$.

B.2 Observables in dimensionless units

B.2.1 Dimensionless momentum density

The momentum density in one dimension is given by

$$p = -\frac{\mathrm{i}\hbar}{2}\left(\psi^*\partial_x\psi - \psi\partial_x\psi^*\right). \tag{B.11}$$

Renormalising the parameter p using $\tilde{p} = p/p_0$ and rewriting the equation using the dimensionless parameters $\tilde{\psi}$ and $\tilde{x}$, gives

$$\tilde{p} = -\frac{\mathrm{i}\hbar n_0}{2x_0p_0}\left(\tilde{\psi}^*\partial_{\tilde{x}}\tilde{\psi} - \tilde{\psi}\partial_{\tilde{x}}\tilde{\psi}^*\right). \tag{B.12}$$

We define the renormalisation constant $p_0 = \hbar n_0/x_0$, which in terms of the healing length and respectively chemical potential reads

$$p_0 = \frac{\hbar n_0}{\sqrt{2}\xi} = n_0\sqrt{m\mu}. \tag{B.13}$$

Substituting $\tilde{p} \to p$, the momentum density in dimensionless units is given by

$$p = -\frac{\mathrm{i}}{2}\left(\psi^*\partial_x\psi - \psi\partial_x\psi^*\right). \tag{B.14}$$

The total momentum P in the system is given by

$$P = \int p dx, \tag{B.15}$$

and is therefore measured in units of $P_0 = \hbar n_0$.

B.2.2 Dimensionless angular momentum

The expectation value of the angular momentum is calculated by

$$\langle L\rangle = -\mathrm{i}\hbar\int \psi^*\partial_\theta\psi dx. \tag{B.16}$$

Assuming an annular trap we can also integrate over the angle rather than space by substituting $dx = Rd\theta$, with R being the radius of the trap. Rewriting the

upper equation using the dimensionless quantities we get

$$\langle L \rangle = -\mathrm{i}\hbar R n_0 \int \tilde{\psi}^* \partial_\theta \tilde{\psi} d\theta. \tag{B.17}$$

By defining $L_0 = 2\pi\hbar R n_0 = \hbar N$, the dimensionless angular momentum is calculated by

$$\langle L \rangle = -\frac{\mathrm{i}}{2\pi} \int \psi^* \partial_\theta \psi d\theta. \tag{B.18}$$

B.3 Dimensionality aspects

While, in three dimensions, the healing length can be written in terms of the s-wave scattering length a as

$$\xi = \frac{1}{\sqrt{8\pi a n_0}}, \qquad \text{using} \qquad g = \frac{4\pi\hbar^2 a}{m} \tag{B.19}$$

this expression does not make sense in lower dimensions [30]. Considering the case of a one-dimensional gas, confined in a cylinder, radially trapped by the harmonic potential $V(r) = (m/2)\omega_\perp^2 r_\perp^2$, the healing length takes the form

$$\xi = \sqrt{\frac{a_\perp^2}{8 a n_0}}, \tag{B.20}$$

where $a_\perp = \sqrt{\hbar/m\omega_\perp}$ is the radial oscillator length.

Appendix C

The program XMDS2

XMDS2 is the acronym for eXtensible Multi Dimensional Simulator. It was developed for the purpose of solving non-linear differential equations by formulating the problem using a high level description written in XML. This code is then converted to C language code and compiled with a C/C++ compiler. That reduces the time of implementing and debugging the code and simultaneously ensures short run times.

The idea of solving differential equations is based on a Fast-Fourier transformation. The original equation is written in Fourier space, solved, and converted back. This method provides a major advantage when solving partial differential equations, since the derivatives are substituted by vectors in k-space and do not have to be calculated explicitly. The underlying principle is explained in the following.

The first order derivative of a function $\psi(x)$ can be written as

$$\partial_x \psi(x) = IFT\left(FT\left(\partial_x \psi(x)\right)\right), \tag{C.1}$$

where FT means the Fourier transformation into k-space and IFT the inverse Fourier transformation. Carrying out $FT(\psi(x))$, yields

$$IFT\left(\int_a^b dx e^{-\mathrm{i}kx}\partial_x\psi(x)\right) = IFT\left(\psi(x)e^{-\mathrm{i}kx}|_a^b + \mathrm{i}k\int_a^b dx e^{-\mathrm{i}kx}\psi(x)\right) \tag{C.2}$$

The first term on the right hand side of the upper equation vanishes because of the periodic boundary conditions while the second one can be identified as the Fourier transformation of the function $\psi(x)$. Therefore equation (C.1) can be

written as

$$\partial_x \psi(x) = \mathrm{IFT}\left(\mathrm{i}k\mathrm{FT}(\psi(x))\right). \tag{C.3}$$

That means that the Fourier transform of an arbitrary n^{th} order derivative can be written as

$$\mathrm{FT}\left(\partial_x^n \psi(x)\right) = (\mathrm{i}k)^n \mathrm{FT}\left(\psi(x)\right). \tag{C.4}$$

Practically that means, every differential operator $L = \partial/\partial x$ has to be replaced by $L = \mathrm{i}k$.

To give the reader an impression of what the coding looks like in Xmds2 we include the following piece of code. We calculate the ground state of a rotating, ring shaped condensate within Gross-Pitaevskii theory using imaginary time propagation. The wave function is renormalised after each time step.

```
<?xml version="1.0" encoding="UTF-8"?>
<simulation xmds-version="2">
  <name>ring</name>
  <author>Gabriele Jaritz</author>

  <features>
    <auto_vectorise />
    <benchmark />
    <bing />
    <fftw plan="exhaustive" />

    <!-- Defining some global variables -->
    <globals>
      <![CDATA[
        const real Omega = 0.4, R = 2.5, Nparticles =6.2832;
        const int C1 = 512;
      ]]>
    </globals>
  </features>

  <!-- Defining the propagation dimension and the transverse dimension -->
  <geometry>
    <propagation_dimension> t </propagation_dimension>
    <transverse_dimensions>
      <dimension name="theta" lattice="512" domain="(0,6.2832)" />
    </transverse_dimensions>
  </geometry>

  <!-- Here we initialising the wave function -->
  <vector name="wavefunctions" initial_space="theta" type="complex">
    <components> psi</components>
    <initialisation>
```

```
    <![CDATA[
      psi = 0.0;
      for (int n=1; n <= C1; n++)
        {
            psi = psi + exp(i*theta*(n-1));
        }
     ]]>
  </initialisation>
</vector>

<!-- We calculating the current normalisation of the wave function
  using the "computed_vector" element -->
<computed_vector name="normalisation" dimensions="" type="real">
  <components> Ncalc</components>
  <evaluation>
    <dependencies basis="theta">wavefunctions</dependencies>
    <![CDATA[
      Ncalc = mod2(psi);
    ]]>
  </evaluation>
</computed_vector>

 <sequence>

 <!-- Normalising the wave function using a "filter" element -->
  <filter>
      <dependencies>normalisation wavefunctions</dependencies>
    <![CDATA[
      psi *= sqrt(Nparticles/Ncalc);
    ]]>
  </filter>

  <!-- Choosing the algorithm and the propagation time. The number in
   the "sample" element defines the length of the output vector -->
  <integrate algorithm="ARK45" interval="100.0" tolerance="1e-12">
    <samples>1600</samples>
    <filters where="step end">
      <filter>
        <dependencies>wavefunctions normalisation</dependencies>
        <![CDATA[
          psi *= sqrt(Nparticles/Ncalc);
        ]]>
      </filter>
    </filters>

   <!--  Defining the operators and differential equation we want
    to solve. The transverse variable in Fourier space is addressed
    by ktheta. The derivative along the propagation dimension t has
    to be written as dpsi_dt -->
    <operators>
      <operator kind="ex" constant="yes">
        <operator_names>T L</operator_names>
```

```
        <![CDATA[
          double k2 = -ktheta*ktheta*0.5;
          T = 1/pow(R,2)*k2;
          L = i*ktheta;
        ]]>
      </operator>

      <integration_vectors>wavefunctions</integration_vectors>
      <![CDATA[
      dpsi_dt = T[psi] - i*Omega*L[psi] - mod2(psi)*psi + psi;
      ]]>
    </operators>
  </integrate>
 </sequence>

 <!-- Defining the output format and variables that are stored -->
 <output format="hdf5" filename="ring.xsil">
  <group>
    <sampling basis="theta" initial_sample="yes">
      <moments>real_psi  imag_psi</moments>
      <dependencies>wavefunctions</dependencies>
      <![CDATA[
      real_psi = Re(psi);
      imag_psi = Im(psi);
       ]]>
    </sampling>
  </group>

 </output>
</simulation>
```

Further useful information about the program package together with a lot of very helpful examples can be found on the web page of reference [54].

Bibliography

[1] F. London. On the Bose-Einstein condensation. *Phys. Rev.*, 54:947–954, 1938.

[2] C.C. Bradley, A. Sackett, J.J. Tollett, and R.G. Hulet. Evidence of Bose-Einstein condensation in an atomic gas with attractive interactions. *Phys. Rev. Lett*, 75:1687–1690, 1995.

[3] O. Fialko, A. S. Bradley, and J. Brand. Quantum tunneling of a vortex between two pinning potentials. *Phys. Rev. Lett.*, 108:015301, 2012.

[4] Claude N. Cohen-Tannoudji. Nobel lecture: Manipulating atoms with photons. *Rev. Mod. Phys.*, 70:707–719, 1998.

[5] J. Stenger, D.M. Stamper-Kurn, M.R. Andrews, S. Chikkatur, S. Inouye, H.-J. Miesner, and W. Ketterle. Optically confined Bose-Einstein condensates. *J. Low Temp. Phys.*, 113:167–188, 1998.

[6] P.C. Hohenberg. Existence of long-range order in one and two dimensions. *Phys. Rev.*, 158:383–386, 1967.

[7] Elliott H. Lieb and Werner Liniger. Exact analysis of an interacting Bose gas. i. the general solution and the ground state. *Phys. Rev.*, 130:1605–1616, 1963.

[8] Elliott H. Lieb. Exact analysis of an interacting Bose gas. ii. the excitation spectrum. *Phys. Rev.*, 130:1616–1624, 1963.

[9] A. Görlitz, J. M. Vogels, A. E. Leanhardt, C. Raman, T. L. Gustavson, J. R. Abo-Shaeer, A. P. Chikkatur, S. Gupta, S. Inouye, T. Rosenband, and W. Ketterle. Realization of Bose-Einstein condensates in lower dimensions. *Phys. Rev. Lett.*, 87:130402, 2001.

[10] H. Ott, J. Fortagh, G. Schlotterbeck, A. Grossmann, and C. Zimmermann. Bose-Einstein condensation in a surface microtrap. *Phys. Rev. Lett.*, 87:230401, 2001.

[11] L. Feenstra, L. M. Andersson, and J. Schmiedmayer. Microtraps and atom chips: Toolboxes for cold atom physics. *General Relativity and Gravitation*, 36:2317–2329, 2004.

[12] M. R. Andrews, C. G. Townsend, H.-J. Miesner, D. S. Durfee, D. M. Kurn, and W. Ketterle. Observation of interference between two Bose condensates. *Science*, 275:637–641, 1997.

[13] Y. Shin, M. Saba, T. A. Pasquini, W. Ketterle, D. E. Pritchard, and A. E. Leanhardt. Atom interferometry with Bose-Einstein condensates in a double-well potential. *Phys. Rev. Lett.*, 92:050405, 2004.

[14] Y. Shin, M. Saba, A. Schirotzek, T. A. Pasquini, A. E. Leanhardt, D. E. Pritchard, and W. Ketterle. Distillation of Bose-Einstein condensates in a double-well potential. *Phys. Rev. Lett.*, 92:150401, 2004.

[15] S. Hofferberth, I. Lesanovsky, B. Fischer, Schumm T., and J. Schmiedmayer. Non-equilibrium coherence dynamics in one-dimensional Bose gases. *Nature*, 449:324–327, 2007.

[16] T. Betz, S. Manz, R. Bücker, T. Berrada, Ch. Koller, G. Kazakov, I. E. Mazets, H.-P. Stimming, A. Perrin, T. Schumm, and J. Schmiedmayer. Two-point phase correlations of a one-dimensional bosonic Josephson junction. *Phys. Rev. Lett.*, 106:020407, 2011.

[17] B.D. Josephson. Possible new effects in superconductive tunnelling. *Phys. Rev.*, 1:251, 1962.

[18] A. Barone and G. Paterno. *Physics and Applications of the Josephson effect*. John Wiley and Sons, 1982.

[19] A.V. Ustinov. Solitons in Josephson junctions. *Physica D*, 123:315, 1998.

[20] A. Smerzi, S. Fantoni, S. Giovanazzi, and S. R. Shenoy. Quantum coherent atomic tunneling between two trapped Bose-Einstein condensates. *Phys. Rev. Lett.*, 79:4950–4953, 1997.

[21] S. Raghavan, A. Smerzi, S. Fantoni, and S. R. Shenoy. Coherent oscillations between two weakly coupled Bose-Einstein condensates: Josephson effects, π oscillations, and macroscopic quantum self-trapping. *Phys. Rev. A*, 59:620–633, 1999.

[22] S. Giovanazzi, A. Smerzi, and S. Fantoni. Josephson effects in dilute Bose-Einstein condensates. *Phys. Rev. Lett.*, 84:4521–4524, 2000.

[23] M. Albiez, R. Gati, J. Fölling, S. Hunsmann, M. Cristiani, and M. Oberthaler. Direct observation of tunneling and nonlinear self-trapping in a single bosonic Josephson junction. *Phys. Rev. Lett.*, 95, 2005.

[24] S. Levy, E. Lahoud, I. Shomroni, and J. Steinhauer. The a.c. and d.c. Josephson effects in a Bose-Einstein condensate. *Nature*, 449:779, 2007.

[25] V. M. Kaurov and A. B. Kuklov. Josephson vortex between two atomic Bose-Einstein condensates. *Phys. Rev. A*, 71:011601, 2005.

[26] V. M. Kaurov and A. B. Kuklov. Atomic Josephson vortices. *Phys. Rev. A*, 73:013627, 2006.

[27] M.I. Qadir, H. Susanto, and P.C. Matthews. Fluxon analogues and dark solitons in linearly coupled Bose-Einstein condensates. *J. Phys. B*, 45:35004–35011, 2012.

[28] I. Bouchoule. Modulational instabilities in Josephson oscillations of elongated coupled condensates. *Eur.Phys.J.D*, 35:147–154, 2005.

[29] R. Hipolito and A. Polkovnikov. Breakdown of macroscopic quantum self-trapping in coupled mesoscopic one-dimensional Bose gases. *Phys. Rev. A*, 81:013621, 2010.

[30] L. Pitaevskii and S. Stringari. *Bose-Einstein Condensation*. Oxford University Press, 2003.

[31] C.J. Pethick and H. Smith. *Bose-Einstein Condensation in Dilute Gases*. Cambridge University Press, 2002.

[32] A.J. Leggett. *Quantum Liquids*. Oxford University Press, 2006.

[33] M. J. Steel, M. K. Olsen, L. I. Plimak, P. D. Drummond, S. M. Tan, M. J. Collett, D. F. Walls, and R. Graham. Dynamical quantum noise in trapped Bose-Einstein condensates. *Phys. Rev. A*, 58:4824–4835, 1998.

[34] C.W. Gardiner and P. Zoller. *Quantum noise*. Springer, 2004.

[35] A. Sinatra, C. Lobo, and Y. Castin. The truncated Wigner method for Bose condensed gases: limits of validity and applications. *J. Phys. B: At. Mol. Opt. Phys.*, 35:3599, 2002.

[36] P.B. Blakie, A.S. Bradley, M.J. Davis, R.J. Ballagh, and C.W. Gardiner. Dynamics and statistical mechanics of ultra-cold Bose gases using c-field techniques. *Adv. Phys.*, 57(5):363–455, 2008.

[37] A. Polkovnikov. Phase space representation of quantum dynamics. *Ann. Phys.*, 325(8):1790 – 1852, 2010.

[38] J. Brand, T. J. Haigh, and U. Zülicke. Sign of coupling in barrier-separated Bose-Einstein condensates and stability of double-ring systems. *Phys. Rev. A*, 81:025602, 2010.

[39] Kerson Huang and C. N. Yang. Quantum-mechanical many-body problem with hard-sphere interaction. *Phys. Rev.*, 105:767–775, 1957.

[40] Anthony J. Leggett. Bose-Einstein condensation in the alkali gases: Some fundamental concepts. *Rev. Mod. Phys.*, 73:307–356, 2001.

[41] M. Olshanii. Atomic scattering in the presence of an external confinement and a gas of impenetrable bosons. *Phys. Rev. Lett.*, 81:938–941, 1998.

[42] T Tsuzuki. Nonlinear waves in the Pitaevskii-Gross equation. *J. Low Temp. Phys.*, 4:441–457, 1971.

[43] R. Kaiser, C. Westbrook, and F. David. *Coherent atomic matter waves - Ondes de matiere coherentes: 27 July - 27 August 1999*. Les Houches - Ecole D'Ete de Physique Theorique. Springer London, Limited, 2007.

[44] A.G. Sykes. *A study of one dimensional quantum gases*. PhD thesis, The Univerity of Queensland, 2009.

[45] N. Rosen and Philip M. Morse. On the vibrations of polyatomic molecules. *Phys. Rev.*, 42:210–217, Oct 1932.

[46] L.D. Landau and E.M. Lifschitz. *Lehrbuch der theoretischen Physik*. Akademie-Verlag Berlin, 1979.

[47] Rina Kanamoto, Lincoln D. Carr, and Masahito Ueda. Topological winding and unwinding in metastable Bose-Einstein condensates. *Phys. Rev. Lett.*, 100:060401, 2008.

[48] A. O. Caldeira and A. J. Leggett. Influence of dissipation on quantum tunneling in macroscopic systems. *Phys. Rev. Lett.*, 46:211–214, 1981.

[49] Jérémie Szeftel. Absorbing boundary conditions for one-dimensional nonlinear Schrödinger equations. *Numerische Mathematik*, 104:103–127, 2006.

[50] Zhenli Xu and Houde Han. Absorbing boundary conditions for nonlinear Schrödinger equations. *Phys. Rev. E*, 74:037704, 2006.

[51] C Farrell and U Leonhardt. The perfectly matched layer in numerical simulations of nonlinear and matter waves. *J. Opt. B*, 7(1):1, 2005.

[52] J. Brand, T. J. Haigh, and U. Zülicke. Rotational fluxons of Bose-Einstein condensates in coplanar double-ring traps. *Phys. Rev. A*, 80:011602, 2009.

[53] C.G. Broyden. A class of methods for solving nonlinear simultaneous equations. *Mathematics of Computation*, 19:577–593, 1965.

[54] G. Dennis, J. Hope, and M. Johnsson. Welcome to the documentation for xmds2!, May 2012. URL http://www.xmds.org/index.html.